Journal of Asian Earth Sciences 193 (2020) 104305

Contents lists available at ScienceDirect

Journal of Asian Earth Sciences

journal homepage: www.elsevier.com/locate/jseaes

Paleomagnetism of the Miocene Soma basin and its structural implications on the central sector of a crustal-scale transfer zone in western Anatolia (Turkey)

Jan Westerweel[a], Bora Uzel[b,*], Cornelis G. Langereis[a], Nuretdin Kaymakci[c], Hasan Sözbilir[b]

[a] Utrecht University, Fort Hoofddijk Paleomagnetic Laboratory, 3584-CD Utrecht, the Netherlands
[b] Dokuz Eylül University, Department of Geological Engineering, TR-35160 İzmir, Turkey
[c] Middle East Technical University, Department of Geological Engineering, TR-06531 Ankara, Turkey

ARTICLE INFO

Keywords:
Paleomagnetism
Kinematic analysis
Anisotropy of magnetic susceptibility (AMS)
Neogene Soma basin
İzmir-Balıkesir Transfer Zone
Western Anatolia

ABSTRACT

The İzmir–Balıkesir Transfer Zone (İBTZ) is a crustal-scale major tectonic feature in western Anatolia accommodating differential extension between the Menderes (MCC) and Cycladic (CCC) core complexes. The kinematics and evolution of the southern part of the İBTZ are well constrained, but its northern continuation remains unstudied. This part is crucial in understanding the complete evolution of western Anatolian tectonics, as well as a possible link between the İBTZ and North Anatolian Fault Zone (NAFZ). In this study, new and extensive paleomagnetic, structural, and stratigraphic data were collected from the Soma basin. These results show that the basin evolved as a part of the İBTZ, including two separate rotational phases. During the first (middle Miocene) phase, deformation was characterized by transcurrent tectonics and associated block rotations as much as ~50° clockwise, during which the İBTZ evolved as a wide dextral shear zone. During the second (late Miocene – recent) phase, the mode of deformation in the Aegean region switched from localized to distributed extension, related to the acceleration of the tearing-off of the African Oceanic slab below the Aegean region. This led to the narrowing of the İBTZ as a discrete brittle shear around the Soma basin, manifested by decoupling of dextral strike-slip and normal faulting. In this period, the Soma basin underwent around −21° counter-clockwise rotation. Based on our new results, the İBTZ extends further to the north and possibly interacts with the southern branch of the NAFZ since the late Miocene.

1. Introduction

The unique position of western Anatolia (Fig. 1a) in the African-European convergent tectonic setting has resulted in a complex deformation history with several large-scale tectonic features. The region is dominated by NNE directed extensional deformation since the late Eocene (Forster and Lister, 2009; Gautier et al., 1999; Jolivet and Brun, 2010; Tirel et al., 2009; van Hinsbergen and Schmid, 2012). There are two major hypotheses to explain the interplay between this extension and the observed tectonic features. One hypothesis is the westward escape of Anatolia (Dewey et al., 1986; Şengör, 1979; Şengör and Yılmaz, 1981; Şengör et al., 1985). This process could have led to the formation of the dextral North Anatolian Fault Zone (NAFZ), as well as of the sinistral East Anatolian Fault Zone along which the Anatolian Block moves westwards. The second hypothesis is related to the rollback of the north-eastward subducting Aegean slab and resulting back-arc extension (Biryol et al., 2011; Le Pichon and Angelier, 1979; Meulenkamp et al., 1988; van Hinsbergen et al., 2005; van Hinsbergen et al., 2010b). Several studies have combined these two hypotheses, suggesting that rollback of the Aegean slab could have been a cause for the westward escape of Anatolia (Bozkurt, 2001; Brun et al., 2016).

In any case, Cenozoic extension in western Anatolia has resulted in two regional extensional features, namely the Cycladic (CCC) and Menderes (MCC) metamorphic core complexes. Moreover, another tectonic feature, the İzmir-Balıkesir Transfer Zone (İBTZ), initiated in between the MCC and CCC, and south of the NAFZ. The İBTZ was first identified by Kaya (1981), who divided the region between İzmir and Balıkesir into several NNE-trending Neogene depressions bounded by oblique-slip faults with a considerable strike-slip component. Şengör (1987) proposed that one of these major NE trending strike-slip cross-faults, located at the western boundary of the Kocaçay basin, offset the main Gediz detachment fault near its western end, and delineated it as a transfer fault zone. After these contributions, Okay and Siyako (1993) have suggested that this whole NE-SW trending zone was the

* Corresponding author.
E-mail address: bora.uzel@deu.edu.tr (B. Uzel).

https://doi.org/10.1016/j.jseaes.2020.104305
Received 2 June 2019; Received in revised form 20 February 2020; Accepted 22 February 2020
Available online 25 February 2020

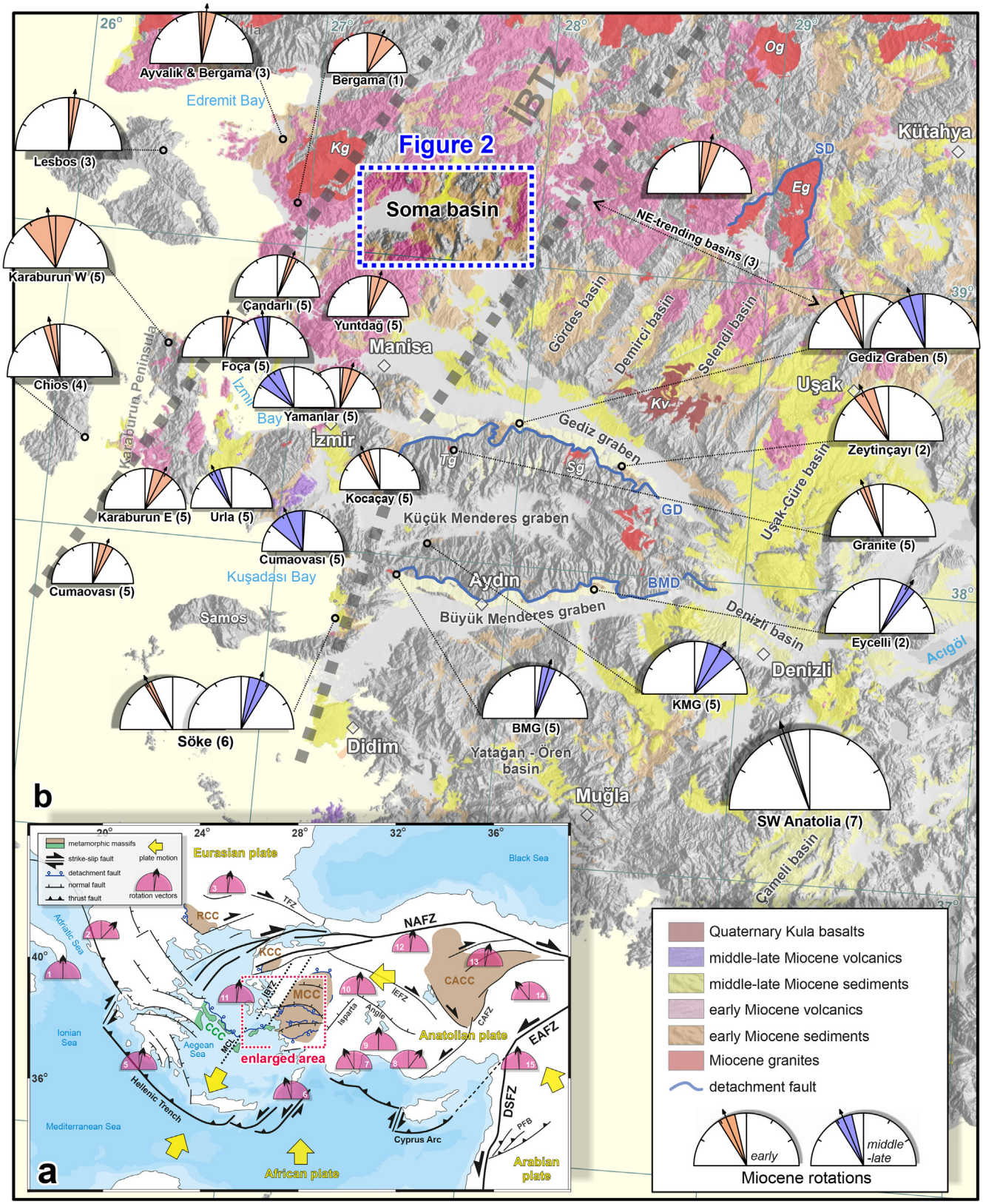

Fig. 1. (a) Large scale tectonic setting of Anatolia (after Kaymakci et al., 2007; Koçyiğit and Özacar, 2003; Taymaz et al., 2007; Uzel et al., 2013); (b) Miocene paleomagnetic results in western and southwestern Anatolia from previous studies. Numbers refer to (1) Kissel et al. (1987), (2) Şen and Seyitoğlu (2009), (3) van Hinsbergen et al. (2010b), (4) Kaymakci et al. (2007), (5) Uzel et al. (2015), (6) Uzel et al. (2017), (7) Kaymakcı et al. (2018). The main structures of western Anatolia are indicated as well. The Soma basin (study area of this research) is highlighted (details in Fig. 2). Abbreviations: GD = Gediz Detachment, AFZ = Akşehir fault zone, BMG = Büyük Menderes Graben, BMD = Büyük Menderes Detachment, CAFZ = Central Anatolian fault zone, DB = Demirci Basin, EPF = Ezinepazarı Fault, GG = Gediz Graben, GB = Gördes Basin, İAS = İzmir–Ankara Suture, İBTZ = İzmir–Balıkesir Transfer Zone, İEFZ = İnönü-Eskişehir fault zone, KMG = Küçük Menderes Graben, KP = Kozak Pluton, MCC = Menderes Core Complex, MCL = Mid-Cycladic Lineament, NAFZ = North Anatolian fault zone, SB = Selendi Basin, SD = Simav Detachment, SG = Simav Graben, TFZ = Thrace fault zone, TGZ = Tuz Gölü Fault Zone, UGB = Uşak- Güre Basin.

depositional loci of the Bornova Flysch Zone, a regional olistostrome–mélange belt, during the Late Cretaceous (Erdoğan, 1990; Okay et al., 2012; Sarı, 2012). Recent studies suggest that it has been reactivated as a NE-SW trending shear zone since the Neogene (Erkül et al., 2005;Ersoy et al., 2012a; Morris and Anderson, 1996; Pe-Piper et al., 2002; Philippon et al., 2012, 2014; Ring et al., 1999; Uzel et al., 2013, 2015; Uzel and Sözbilir, 2008; Walcott and White, 1998; Sözbilir et al., 2003). Uzel et al. (2013, 2015) argued that transtensional deformation within this shear zone accommodates differential extensional strain between the CCC and MCC since the Miocene, alongside the Mid-Cycladic Lineament (MCL). The Miocene volcano-sedimentary units and Quaternary continental units exposed in western Anatolia were all deposited and deformed within the İBTZ (Kaya, 1981; Sözbilir et al., 2011; Uzel and Sözbilir, 2008; Uzel et al., 2012, 2013). In addition, Uzel et al. (2015) and Brun et al. (2016) suggested that the İBTZ is a surface expression of a subduction transform edge propagator fault (STEP-fault; Govers and Wortel, 2005), related to a slab tearing of the Aegean slab due to rollback (Erkül et al., 2005, 2013; Uzel et al., 2015). There is a proposed connection between this slab rollback, the İBTZ, and the NAFZ (Gessner et al., 2013; Özkaymak et al., 2013; Uzel et al., 2013). Understanding the northern continuation of the İBTZ and its relationship with the NAFZ is required for a complete knowledge of western Anatolian tectonics, a seismically active region with frequent earthquakes.

In addition, there is another crucial uncertainty in constraining the tectonic history of western Anatolia. Several studies suggested that the Cenozoic extension took place in a single deformation phase (Glodny and Hetzel, 2007; Kaymakci, 2006; Seyitoğlu et al., 2000, 2002, 2004), while others proposed that it occurred during multiple deformation phases, separated by periods of inversion and tectonic quiescence (Beccaletto and Steiner, 2005; Bozkurt, 2001; Bozkurt and Sözbilir, 2004, 2006; Bozkurt and Mittwede, 2005; Emre and Sözbilir 2007; Kaya et al., 2004, 2007; Kaymakci 2006; Koçyiğit et al., 1999; Purvis and Robertson 2004, 2005; Sözbilir, 2001; Yılmaz et al., 2000). The role and evolution of the İBTZ within this tectonic setting were not well understood until recently, as paleomagnetic studies in the Aegean region were not focussed on the IBTZ. Only recently, Uzel et al. (2013, 2015, 2017) conducted structural and paleomagnetic research within the southern part of the İBTZ and adjacent regions (Fig. 1b). They argued that at least three strike-slip dominated deformation phases occurred throughout the İBTZ during the Neogene. Their paleomagnetic data constrained at least two distinct rotational phases separated by a middle Miocene angular unconformity (Uzel et al., 2015, 2017). Deformational and rotational trends within the İBTZ were different from the adjacent CCC and MCC regions. This indicates that the İBTZ evolved as a system of rigid-body rotations related to orthogonal extension (Jolivet and Brun, 2010; Uzel et al., 2015). However, these observations do not completely agree with the conclusions of van Hinsbergen et al. (2010b), who did not recognize the occurrence of rigid-block rotations within parts of the İBTZ and only distinguished one Miocene rotational phase in western Anatolia, related to asymmetrical exhumation of the MCC. Similarly, the data provided by Uzel et al. (2015) also contradict Kondopoulou et al. (2011), who argued that the coastal region of western Anatolia is characterized by a “chaotic pattern” of coexisting clockwise (CW) and counterclockwise (CCW) rotations.

In this context, the next logical step is to investigate the northern continuation of the İBTZ system, since this will provide crucial insight in understanding the connection between the İBTZ and the NAFZ. In this regard, new data will elucidate the relationship between the multiple-phase formation of the İBTZ of Uzel et al. (2013, 2015, 2017) and the single-phase asymmetrical exhumation of the MCC of van Hinsbergen et al. (2010b). Therefore, the goal of this research is to constrain the Neogene deformation history of the Soma basin, western Anatolia, and adjacent regions (Fig. 1). This area is located at a cross-point directly north of the area studied by Uzel et al. (2013, 2015, 2017), directly west of the area studied by van Hinsbergen et al. (2010b) and proximal to the southern strands of the NAFZ. In this contribution, we will present the results of newly acquired paleomagnetic data, as well as new structural and stratigraphic and anisotropy of magnetic susceptibility (AMS) results.

2. Geological setting

Western Anatolia is a region with a complex deformation history, where NNE trending extension and exhumation has taken place since the late Eocene (Şengör et al., 1985). The main geological features of the region are the MCC, the CCC, and the NE-SW trending İBTZ. The Soma basin is one of the basins located within the central part of the İBTZ.

2.1. Menderes core complex (MCC)

The geology of the region directly east of the İBTZ is characterized by the MCC and several E-W to NE-SW trending Neogene basins. The stratigraphy of the MCC consists of two sequences; a high-grade metamorphic core which consists of augen gneisses, metagranites, schists, paragneisses, and metagabbros, and a lower-grade metamorphic cover comprising schists, quartzites, amphibolites, phyllites, and marbles. Its metamorphism history can be traced back to late Proterozoic to early Paleozoic Pan-African events as well as to Mesozoic to Cenozoic Alpine orogenic events (Akkök, 1983; Bozkurt and Park, 1997; Candan et al., 1997, 2001; Okay, 2001).

The NE-SW trending basins in the northern part of the MCC are often called the Northern Menderes Massif basins. The largest of these are from west to east the Gördes, Demirci, Selendi, and Uşak-Güre basins (Şengör, 1987; Yılmaz et al., 2000). The basins are bounded on their northern and southern margins by E-W trending detachment faults as well as high angle normal faults. On their eastern and western margins, the basins are bounded by dextral or sinistral strike-slip faults, which were interpreted by Şengör (1987) as cross-faults related to the differential extension. Therefore, most of these basins have been interpreted as upper crustal supradetachment basins related to rapid, NNE-SSW trending extension of young, hot crust, resulting in domal uplift and exhumation of the crustal-scale MCC during the Oligocene-Miocene (Bozkurt, 2000; Bozkurt and Sözbilir, 2006; Çiftçi and Bozkurt, 2009; Koçyiğit et al., 1999; Sözbilir, 2001, 2002). According to van Hinsbergen et al. (2010b), this exhumation occurred asymmetrically with the Büyük Menderes and Gediz detachments defining a pivot point, separating CW rotation in the north and CCW rotation in the south.

2.2. Cycladic core complex (CCC)

The CCC and related detachment faulting are less exposed in western Anatolia compared to the Menderes region. It is mainly exposed in the southern margin of the Kocaçay Basin (Sözbilir et al., 2011) in a crescent-shape belt that extends into adjacent Greek islands such as Samos and Ikaria. The main event that influenced the CCC was the Aegean subduction during the Eocene, which resulted in high-pressure metamorphism (Jolivet and Brun, 2010). In some places, high-temperature metamorphism superimposed high-pressure metamorphism (Brun et al., 2016; Philippon et al. 2012). The main rocks that comprise the CCC are mica- and calc-schists, marbles, meta-cherts, serpentinites, and meta-volcanic rocks in western Anatolia (Okay, 2001; Sözbilir et al., 2011). Like the MCC, the exhumation of the CCC took place during the Oligocene-Miocene (Vandenberg and Lister, 1996). It is cross-cut by basins with a progressively more continental sedimentary infill of similar age separated by large-scale detachments, comparable to the MCC (Brun et al., 2016). The CCC has experienced a greater degree of extension since the Eocene compared to the MCC (Gessner et al., 2013; Ring et al., 1999; Uzel et al., 2013).

2.3. İzmir-Balıkesir Transfer Zone (İBTZ)

The İBTZ was recognized in many studies as a NE-SW trending transtensional shear zone, accommodating differential extension between the MCC and CCC (Erkül et al., 2005; Ring et al., 1999; Uzel and Sözbilir, 2008; Sözbilir et al., 2011; Uzel et al., 2013, 2015). It is dominated by strike-slip deformation from the Miocene onwards, as evidenced by GPS data and earthquake focal mechanisms (Aktuğ and Kılıçoğlu, 2006; İnan et al., 2012; Uzel et al., 2013; Zhu et al., 2006). It has been suggested that the İBTZ is a surface expression of a slab-tear induced by the rollback of the Aegean slab (Uzel et al. 2015). This slab-tear forms a lateral boundary of the Hellenic trench system. Mantle windows often coincide with the location of the slab edge developed during the formation of a slab-tear (Biryol et al., 2011; Govers and Wortel, 2005; Jolivet et al., 2013; van Hinsbergen et al., 2010a). According to results from tomography (Biryol et al., 2011; Paul et al., 2014; van Hinsbergen et al., 2010a), surface observations (Gessner et al., 2013; Ring et al., 1999; Erkül et al., 2005, 2013; Uzel et al., 2013, 2015) and geochemistry (Aldanmaz et al., 2000; Altunkaynak et al., 2010; Ersoy et al., 2012a; Pe-Piper et al., 2002; Karacik et al., 2013), there is indeed evidence for such a mantle window, adding further credibility to the hypothesis that the İBTZ is a surface expression of a slab-tear. The formation of the İBTZ is also manifested by corresponding NE aligned volcanism (Genç et al., 2001; Uzel and Sözbilir, 2008; Sözbilir et al., 2011). Previous studies constrained at least three deformation phases (Uzel et al., 2013) and two rotational phases (Uzel et al., 2015, 2017) within the İBTZ (Fig. 1b). The first deformation phase was dominated by NE-SW trending transtension during the early to late Miocene. This led to the formation of NE-SW trending basins within the zone. It has been suggested that these basins follow inherited structural trends (Kaya, 1981). This deformation phase was followed by Pliocene overall pure strike-slip deformation, which coincided with the final exhumation phase of the MCC, the formation of the NAFZ, and the cessation of displacement along the MCL. During the third deformation phase in the late Pliocene-Quaternary, the İBTZ evolved from a wide shear zone into a relatively narrow fault zone. During this phase, extensional and strike-slip deformation were completely decoupled from each other with NW–SE trending sinistral and NE–SW trending dextral strike-slip faults occurring alongside E-W trending normal faults. Extension was oriented NNW–SSE to NNE–SSW during this last phase within the İBTZ (Uzel et al., 2013), while the regional extension was N-S to NE-SW oriented since the Oligocene (Bozkurt, 2003; Bozkurt and Sözbilir, 2004; Lips et al., 2001; Seyitoğlu and Scott, 1996; Sözbilir, 2001).

According to paleomagnetic data by Uzel et al. (2015), the first rotational phase is expressed in early Miocene volcano-sedimentary rocks as an average net 23 $\pm$ 6° CW rotation. This was followed by a reorganization in the rotation pattern during the second phase, which is characterized by an average net rotation of 22 $\pm$ 11° CCW (Uzel et al., 2015). This suggests that the İBTZ region underwent a significant 45° CW rotation in the middle Miocene, followed by a 22° CCW rotation after the late Miocene. In addition, the narrowing of the İBTZ occurred progressively following the first rotational phase.

2.4. Soma basin

The Soma basin is one of the Neogene basins within the İBTZ, developed on the Eocene to Palaeozoic basement (Figs. 1 and 2). Because early studies on the geology of the basin were mainly focused on its abundant coal-bearing deposits, it was thought to be an intramontane basin, which developed in the topographic depressions related to Alpine deformation of the pre-Neogene basement (İnci, 1998, 2002). However, more recent studies suggest that faulting played an important role in the formation of the Soma basin, as it is bounded on all sides by high angle faults and horsts (Arpaliyiğit, 2004). The most recent studies (Uzel and Sözbilir, 2008; Uzel et al., 2012, 2013; Uzel, 2017) provided evidence for the occurrence of both major strike-slip and normal faulting in the İBTZ basins, and therefore they interpret these basins as transtensional strike-slip basins. Overall, the deposits in the Soma basin can be divided into three stratigraphic sequences separated by regional unconformities. These sequences include, from older to younger, (i) pre-Neogene rocks, (ii) Neogene volcano-sedimentary units, and (iii) Plio-Quaternary units (Arpaliyiğit, 2004; İnci, 2002; Kaya et al., 2004; Özkaymak et al., 2013). The focus of this research will be on the Miocene volcano-sedimentary units (Fig. 3) since they were deposited and deformed during the main tectonic events that formed the İBTZ.

2.4.1. Neogene volcano-sedimentary units

The base of the Miocene volcano-sedimentary sequence is characterized by alluvial fan conglomerates deposited along the basin margins, derived from the adjacent topographic highs that consist of basement lithologies (İnci, 2002). Uzel et al. (2017) concluded that an erosional period took place during the middle Miocene, and this hiatus is hence called the Middle Miocene Unconformity (MMU). It divides the Miocene volcano-sedimentary rocks into a lower and upper sequence (Fig. 3). In the Soma basin, the lower sequence is called the Soma Formation, while the upper sequence is named as Deniş Formation (Nebert, 1978; İnci, 2002). Our observations indicate that the Soma Formation consists mainly of limestones alternating with sandstones, siltstones, and marls. These deposits are intercalated with organic-rich, coal-bearing layers as well as pyroclastic, biotite- and plagioclase-rich tuff and tuffite deposits. Grey to white marl is the most abundant lithology in both the lower and the upper sequence in the basin. Occasional gastropod-rich marlstone deposits are present as well. Organic-rich layers contain fossil leaves, while common sedimentary structures are mud cracks and load casts. The dominant environment was fluvio-lacustrine throughout the deposition of the Soma and Deniş formations (İnci, 2002).

According to our field observations and revised stratigraphy of the area, these two formations are separated from each other by the Yuntdağ volcanics (Fig. 3), which formed as a NE-SW trending volcanic ridge within the İBTZ during the early Miocene (21.0–15.9 Ma, Borsi et al., 1972; Ercan et al., 1996; Ersoy et al., 2012b; Uzel et al., 2020). We subdivided the volcanic rocks of the Soma basin into two categories: (i) pinkish to greyish, porphyritic, biotite- and plagioclase-rich andesites and rhyolites and (ii) grey to black, aphanitic olivine bearing basalts and trachybasalts, which sometimes form columnar joints. Both categories can contain empty vesicles, suggesting a subaerial environment during extrusion. The first extrusion identifiable as the Yuntdağ volcanics cover the entire succession of the lower sequence (Fig. 3). In the second phase of volcanism, the Dededağ basalts (Fig. 3), was synchronous with the deposition of the upper sedimentary sequence. According to our field observations, basalt and basaltic andesite lava flows and their pyroclastic deposits are often intercalated with the Deniş Formation. Here, the contact between extrusion and sediment is characterized by baked contacts at the bottom of the lava flow, while no baking took place at the top, ruling out the possibility of a magmatic sill. This second phase of volcanism also covers the upper sequence successions.

2.4.2. Plio-Quaternary units

According to stratigraphic field observations, it appears that the Pliocene Kumköy Formation rests unconformably on the Soma and Deniş Formations (Fig. 3). The Kumköy Formation is hence considered as the sedimentary succession of post-Miocene sedimentation that corresponded to the non-volcanic edifice of the İBTZ in the Soma basin. This formation consists of well-sorted, subrounded to rounded ellipsoidal pebble conglomerates with imbrications, sandstones and mudstones with cross-bedding as well as soft-sediment deformation structures such as load casts and flame structures, and finally pisolite-rich lacustrine carbonates. Collectively, these features indicate that the depositional environment of the Kumköy Formation was an association of

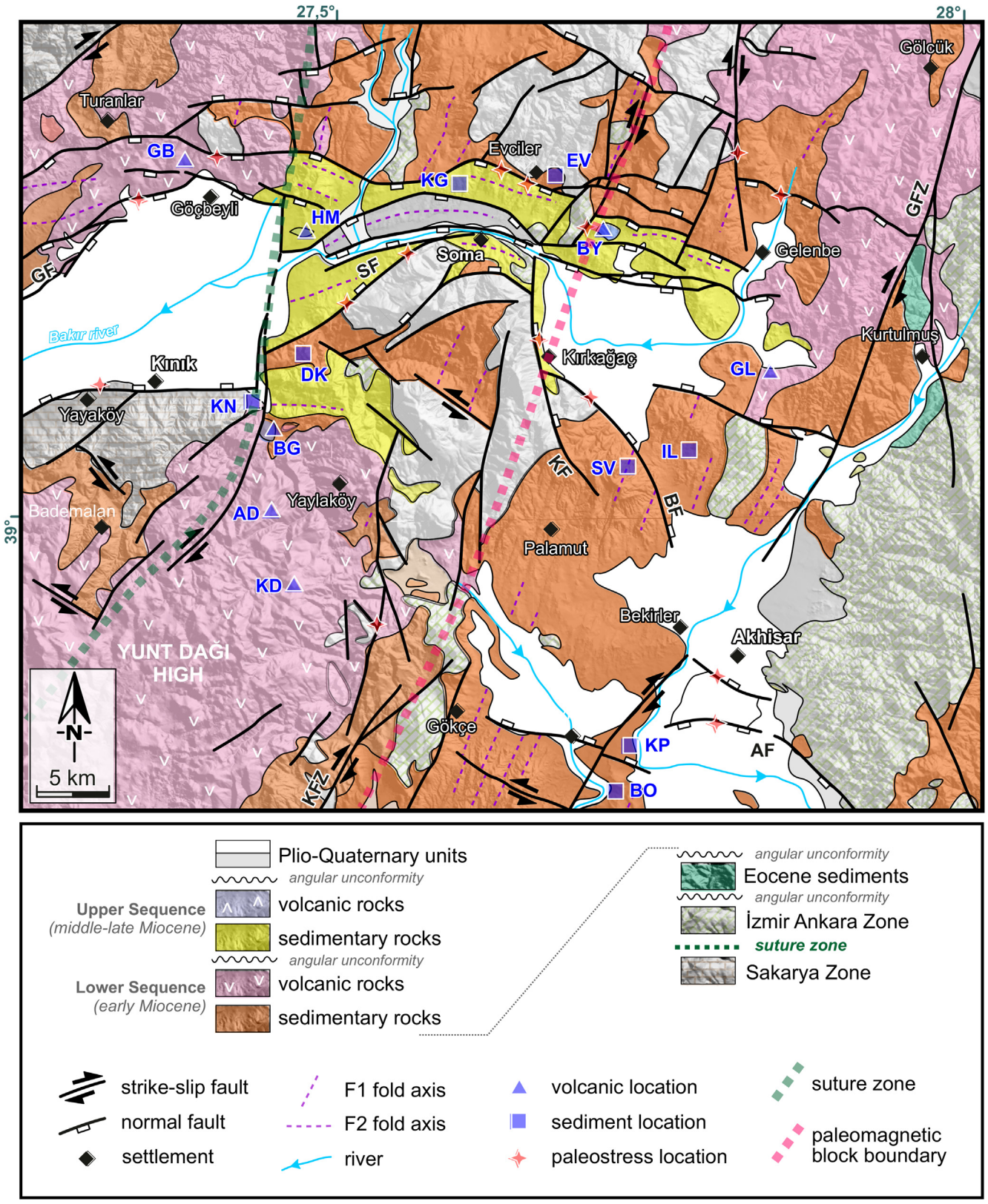

Fig. 2. (a) Geological map of Turkey with the study area of this research and paleomagnetic sampling locations indicated (after Inci, 1998; GDMRE, 2002; and this study). Triangles (squares) denote volcanic (sedimentary) sites, respectively; red stars indicate sites for paleostress measurements. Site abbreviations: AD = Arpadere, BG = Bağalan, BO = Beyoba, BY = Bayat, DK = Dereköy, EV = Evciler, GB = Göçbeyli, GL = Gelembe, HM = Hamidiye, IL = Ilyaslar, KD = Karadere, KG = Küçükgüney, KN = Kınık, KP = Kapaklı, SV = Selvili. Structural abbreviations: AF = Akhisar Fault, BF = Bakır Fault, GFZ = Gelembe Fault Zone, KF = Kırkağaç Fault, KFZ = Kaleköy Fault Zone. (b) rose diagrams prepared from the orientations of folds. Note the orientation of F1 and F2 are almost perpendicular to each other. F1 folds developed as buckle folds while F2 folds are developed as forced folds above normal faults.

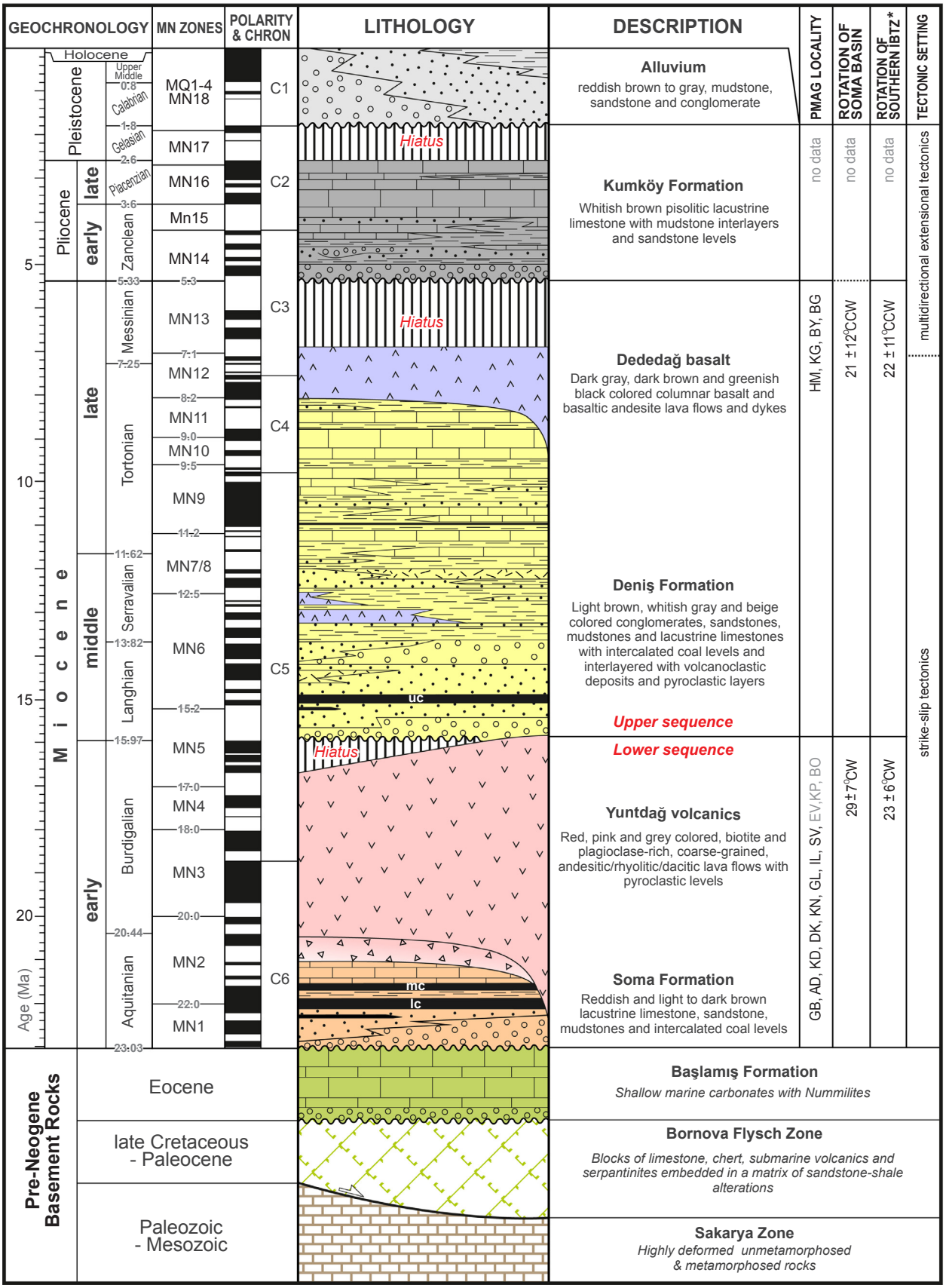

Fig. 3. Integrated stratigraphic column of the Soma basin based on our observations and previous studies (Arpaliyiğit, 2004; İnci, 2002). Rotation data of the IBTZ are from Uzel et al. (2015). The abbreviations of sampling localities are the same as in Fig. 2.

fluvial and lacustrine environments.

The most recent deposits of the Soma basin include Quaternary alluvial deposits developed along present-day streams. They rest unconformably on the older units (Fig. 3). Our observations show that they consist mainly of typical alluvial fan deposits characterized by reddish-brown colluvial fan-apron deposits along with slope breaks and proximal matrix-supported cross-bedded conglomerates and sandstones. The rest of the Quaternary infill of the Soma basin consists of cross-bedded channel conglomerates and sandstones, as well as mudstones. These are typical meandering river deposits, as indicated by their morphology that includes point-bars, a high sinuosity of the river channel, and epsilon cross-bedding in the coarse clastics wherever they are exposed. These sediments contain clasts derived from both the pre-Neogene basement and Neogene volcano-sedimentary units.

2.5. Structural geology

We have updated the 1/25000 scale geological map of the Soma basin in the light of data from İnci (1998) and MTA (2002). The resulting geological map of the study area and the revised stratigraphy are shown in Figs. 2 and 3, respectively. In the sections below, the newly acquired structural and kinematic data from the Soma basin is presented according to the revised stratigraphy of the area (Figs. 4 and 5).

2.5.1. Faults

The faults observed within the Soma basin can be classified into three general groups: NE-SW trending dextral strike-slip faults, NW-SE trending sinistral strike-slip faults, and E-W trending normal faults. These three fault sets are henceforth called D1, S1, and N1 (Fig. 5).

D1 faults are characterized by NE-SW striking fault planes with high dip angles (> 60°) and well-constrained near-horizontal slickenside pitches (Figs. 4a-b and 5). They generally displaced lower sequence units and the basement. The same is true for the NW-SE trending S1 faults. However, S1 faults generally have a larger normal component, as indicated by steeper slickenside pitches. They exhibit less constrained slip directions compared to D1 (Figs. 4c and 5). N1 faults are oriented approximately E-W and have higher dip angles and slickenside pitches compared to D1 and S1 (Fig. 4g). The most notable exceptions on D1 faults are the Bakır and Kirkağaç faults: unlike other E-W trending normal faults, they have N-S to NW-SE strikes and have normal fault characteristics. Most of the N1 faults are cross-cutting the whole sedimentary successions, including Quaternary alluvium, indicating recent activity (Fig. 4f–i). In addition, the N1 faults cut and displace D1 and S1 faults (Fig. 2) except for the Gelembe Fault Zone (GFZ in Fig. 2), a member of D1 group, which displaces all other structures and is still active at present (Emre et al., 2016).

The slip directions and constructed paleostress configurations indicate that the D1 faults were developed under NNW-SSE directed extension and WSW-ESE directed compression (Fig. 4c), while intermediate stress was subvertical (σ_1: 258°N/15°, σ_2: 041°N/72°, σ_3: 165°N/10°). Subvertical intermediate and horizontal major and minor stress orientations indicate that these faults were developed in a transcurrent (strike-slip) tectonic setting along the İBTZ.

A reliable paleostress analysis could not be performed for the S1 faults because the number of fault slip data were not sufficient to

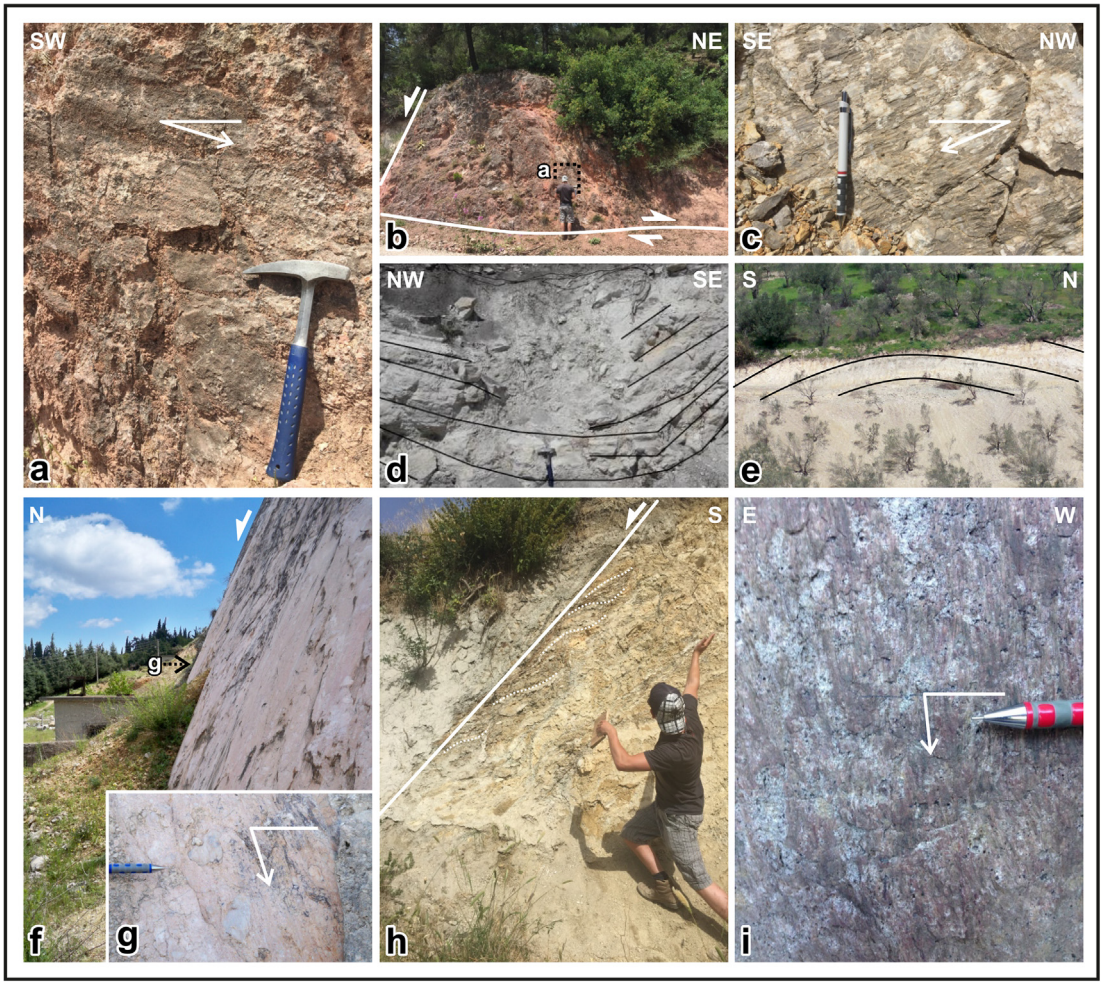

Fig. 4. Representative field photographs of deformational structures of D1 (a, b), S1 (c), F1 (d), F2 (e) and N1 (f-i).

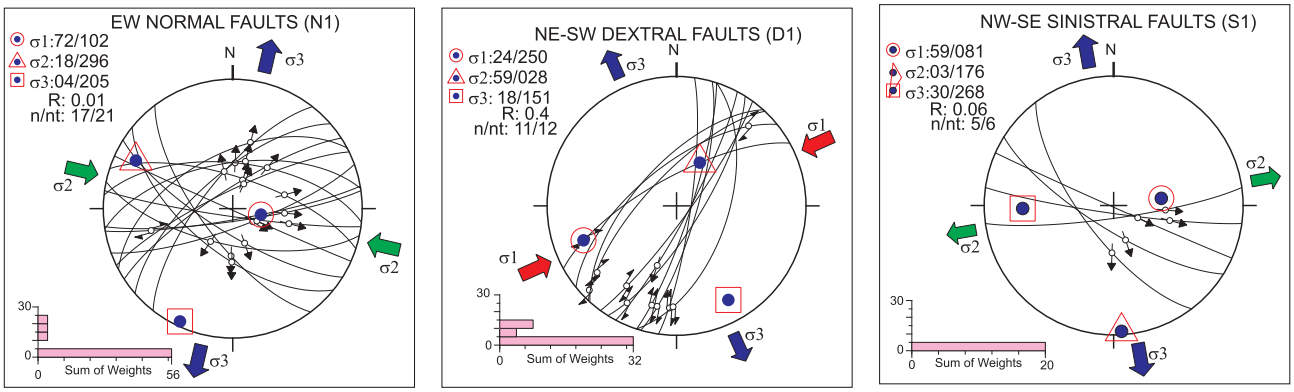

Fig. 5. Paleostress configurations obtained from the faults in the study area using WinTENSOR software (Delvaux and Sperner, 2003). n: number of valid faults used in the inversion after best-fit analysis, nt = the total number of fault-slip data measured in the field, R = ratio of principal stress differences (σ2-σ3)/(σ1-σ3). Sum of weights refers to angular divergence range between obtained orientations and the measured slip directions.

constrain the tectonic setting. Nevertheless, the available data suggest tri-axial strain conditions for S1, as indicated by subhorizontal and subvertical stress orientations (Fig. 4f). Field observations and relative age relationships (cross-cutting with D1 faults) suggest that S1 faulting is most likely a conjugate fault system along the İBTZ.

The paleostress configurations constructed for the N1 fault set indicate that they were formed under approximately N-S extension. Computed kinematic data show that the principal stress axes are oriented as σ_1: 047°N/73°, σ_2: 277°N/11°, σ_3: 184°N/12° (Fig. 4i). As seen in Fig. 4h, the slickensides trend almost radially, indicating uniaxial stress conditions that develop when the magnitudes of two of the stress components (σ_2 and σ_3) are almost equal. The resultant geometry implies a multi-directional extension. If such conditions develop when σ_1 is vertical, such stress conditions tend not to be associated with relative block rotations.

2.5.2. Folds

Two distinct fold axis orientations are present in the Soma basin (Fig. 2). The first set of folds has an approximately NE-SW trend (Fig. 2b), indicating WNW-ESE directed shortening. This fold set is henceforth called F1, and it can be observed in the Neogene volcano-sedimentary units (Fig. 4d). These folds are occasionally cut and displaced by N1 faults across the study area (Fig. 2a).

The second fold set (F2) affected Neogene volcano-sedimentary units, but only within the hanging wall blocks of (N1) normal faults (Fig. 4e). These folds are generally open to gently plunging folds, and their axes are mostly parallel to the nearby E-W trending normal faults (Fig. 2b). These orientations suggest that the region deformed either under N-S directed contraction (Bozkurt, 2000; Bozkurt and Sözbilir, 2004; Bozkurt and Rojay, 2005; Özkaymak et al., 2013), provided that they are buckle folds, or they are forced folds developed in response to normal faulting in the basement, which would indicate N-S extension. Similar to F1 folds, the orientations of the F2 folds are not compatible with the stress conditions that created D1 and S1 faulting. Their close proximity and parallel orientations to the N1 normal faults indicate that F2 folds are bending related forced folds (as opposed to buckle folds) developed in response to N-S directed extension, which also controlled normal faulting. Such a mechanism is already proposed for some of the folds in the Gediz graben (Çiftçi and Bozkurt, 2009; Seyitoğlu et al., 2000; Sözbilir, 2001, 2002) and the Denizli basin (Kaymakci, 2006). According to field observations and geological mapping, the F2 folding was probably formed during or after the late Miocene and is related to the high angle normal (N1) faulting across the Soma basin, while F1 folds developed due to WNW-ESE directed σ_2 since the late Miocene.

3. Methods

3.1. Structural analysis

Field-based structural mapping and kinematic analysis were conducted to investigate the nature and order of deformation that occurred in the Soma basin. The orientations of fault planes and fold axes, as well as cross-cutting relationships, provide constraints on different deformation phases. Kinematic indicators, such as slip lineations (slickoliths, slickensides, slickenfibres, etc.), stratigraphical offset features, and Riedel shear geometries, are used to identify shear sense. The collected fault slip data are used to reconstruct paleostress configurations for each deformation phase. The computations were performed using Win_TENSOR (Delvaux and Sperner, 2003) software. The ranking scheme from Delvaux and Sperner (2003) was applied for checking the quality of the fault slip data. Finally, field observations and geological cross-sections were utilized to determine the relative ages of different structures and lithologies.

3.2. Paleomagnetism

Paleomagnetic analysis of rocks is an effective method for determining the deformation history of strike-slip fault zones with prevailing simple shear conditions, like the İBTZ, because it can constrain vertical-axis rotations with respect to the present-day geographic north (Christie-Blick, 1985; Tauxe, 2010). In addition, analysis of the AMS in sediments provides constraints on paleostress directions for comparison with the structural data (Hrouda, 1982; Tauxe, 2010).

In total, we distinguished 25 early Miocene volcanic sites distributed over four localities: Arpadere (AD), Göçbeyli (GB), and Karadere (KD); and 15 middle-late Miocene volcanic sites from the localities of Bağalan (BG), Gelembe (GL) and Bayat (BY). Furthermore, we distinguished 24 early Miocene sedimentary sites across seven localities: Selvili (SV), İlyaslar (IL), Kınık (KN), Evciler (EV), Dereköy (DK), Beyoba (BO) and Kapaklı (KP); and 17 middle-late Miocene sedimentary sites from the localities of Hamidiye (HM) and Küçükgüney (KG). The distribution of all localities is shown in the geological map of Fig. 2. From these localities, 664 conventional paleomagnetic core plug samples (Ø 25 mm) were collected in stratigraphic order using a gasoline-powered drilling machine, consisting of 338 volcanic and 326 sedimentary samples (Fig. 6).

Volcanic rocks cool relatively fast and therefore retain spot readings of the geomagnetic field, while sedimentary rocks average out paleosecular variation due to relatively slow sedimentation rates. The magnetic signal of sedimentary rocks is overall weaker compared to volcanic rocks. The availability of suitable outcrops determines the sampling distribution for paleomagnetic study. As a result, the sizes and

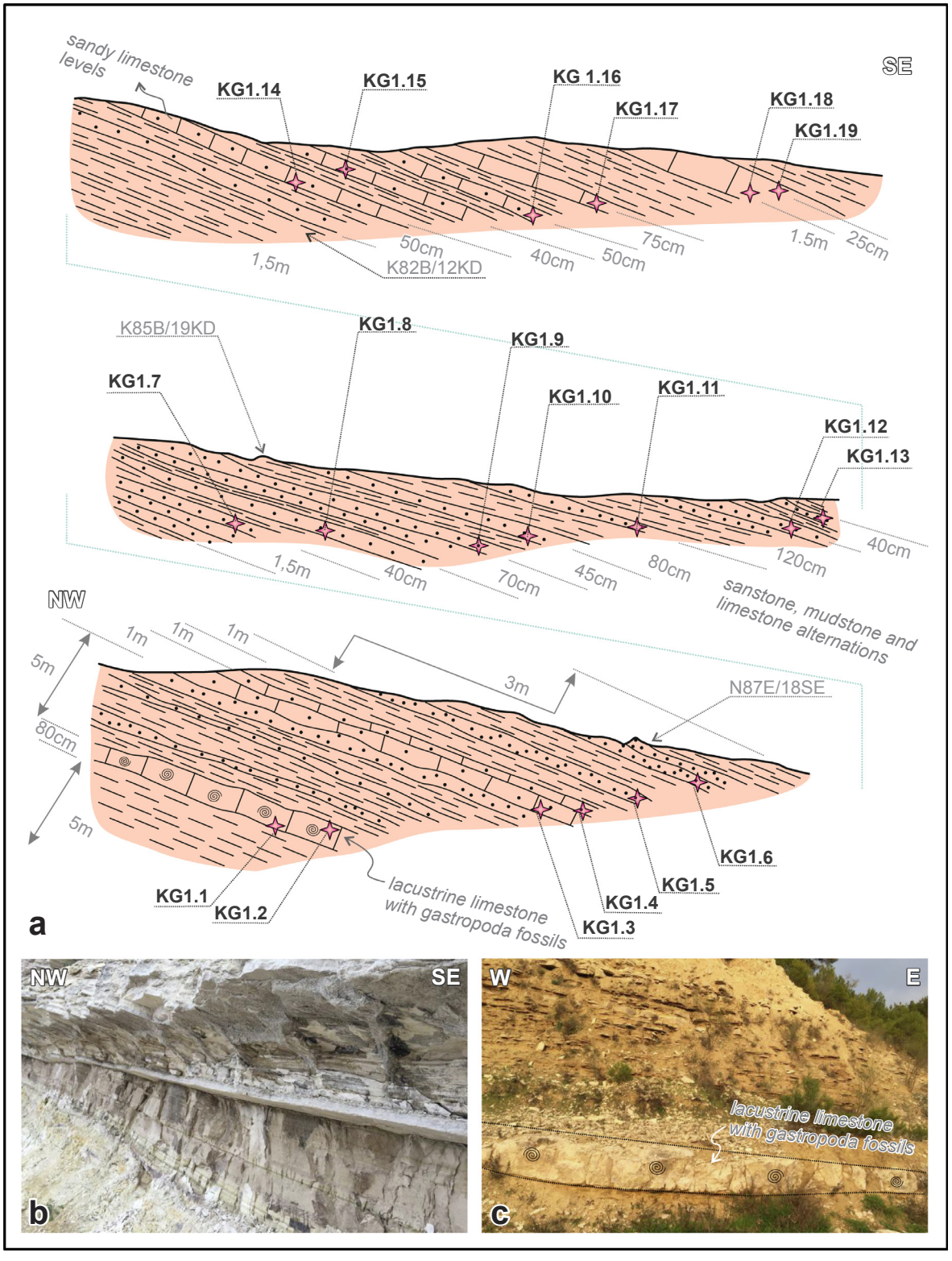

Fig. 6. Geological cross-sections of representative paleomagnetic sampling sites from localities Bağalan (BG), Hamidiye (HM) and Küçükgüney (KG), including lithologies, sampling distribution and field pictures.

boundaries of tectonic blocks are sometimes poorly constrained, which is further complicated by the occurrence of several deformation phases in the study area. For these reasons, several sites from the same volcanic locality were sampled. In addition, all sampled localities are distributed as equally as possible over the study area and over different lithologies. The exception to this is the Soma open coal pit mine, which contained no suitable outcrops due to intense deformation. For measurement purposes, all samples were oriented using a magnetic compass and, if possible, a sun compass for volcanic rocks. Furthermore, the bedding orientation was measured at every site to check whether a geographic or tectonic coordinate system yields more consistent directions. For the volcanic rocks, bedding planes are checked with the closest

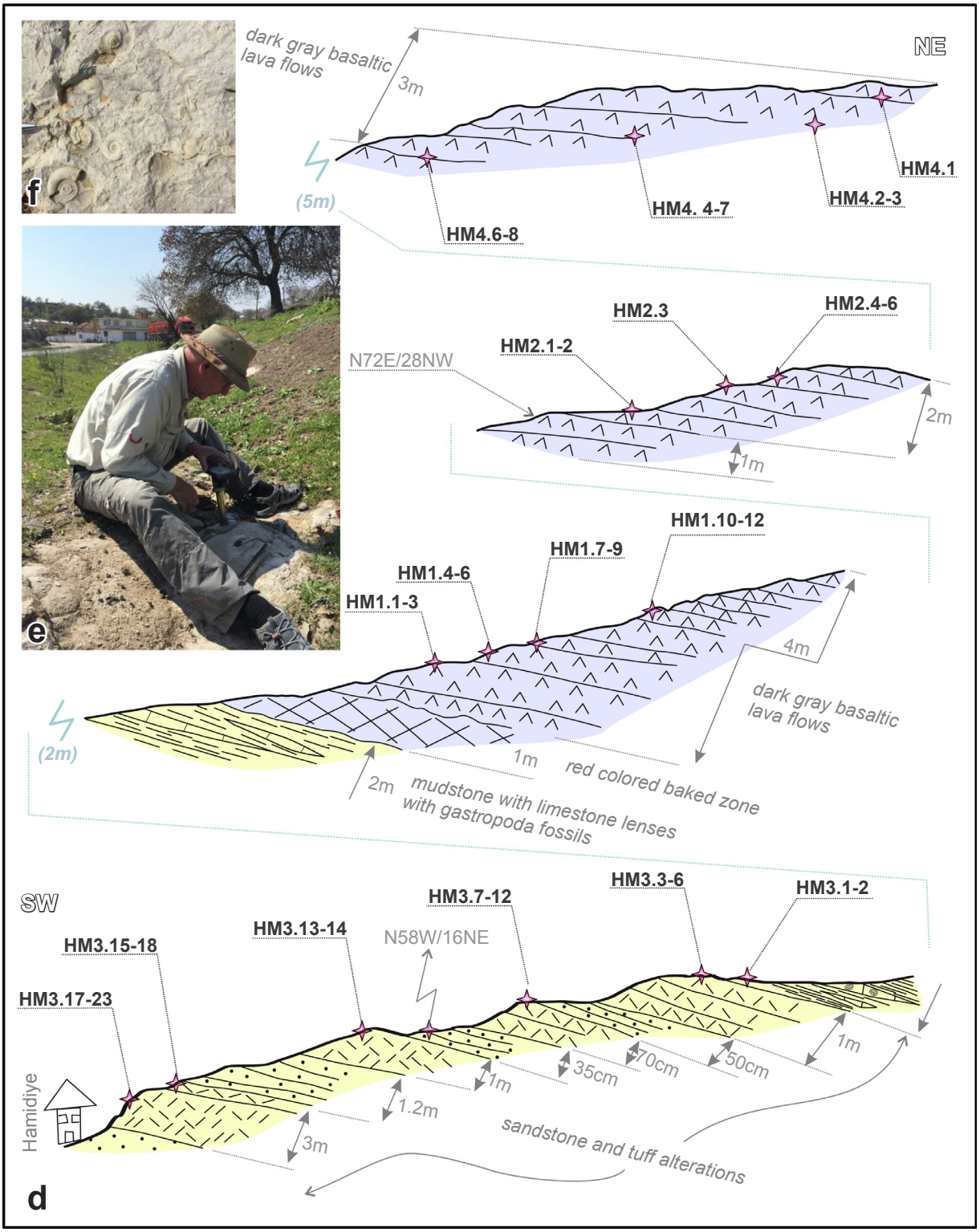

Fig. 6. (*continued*)

sedimentary bedding for the reliability of their paleo-horizontal position whenever possible, although these paleo-horizontal measurements remain prone to errors related to unclear bedding surfaces or the effect of paleo-topography causing non-horizontal deposition of lava flows. Core orientations and bedding strikes were corrected for the declination of the present-day field of ~5° (Thébault et al., 2015). In the laboratory, the cores were cut into 22 mm specimens for sedimentary cores and 11 mm for volcanic cores, because of their overall stronger magnetic signal.

3.2.1. Thermal variation of magnetic susceptibility

The dominant magnetic carriers and chemical alterations of a selection of samples from different localities were determined by measuring their mass-normalized bulk magnetic susceptibility at increasing temperature steps. This was done using an AGICO KLY-3 (noise level $3.2*10^{-13}$ A m^2). The samples were powdered, weighted, and put into a

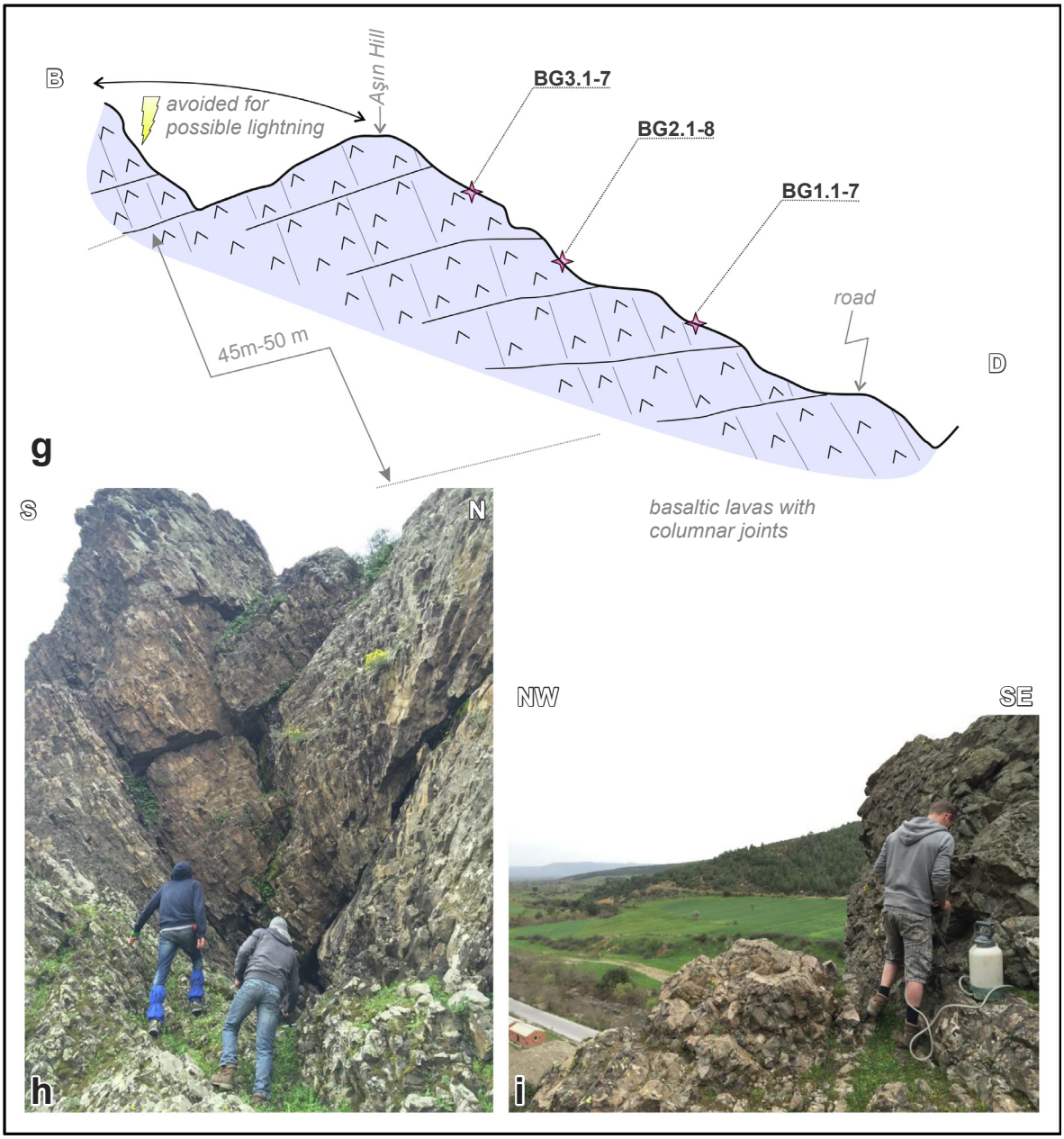

Fig. 6. (*continued*)

quartz-glass sample holder. The mass-normalized bulk magnetic susceptibility was measured during several heating and cooling cycles at steps of 60 °C, starting at 180 °C up to a maximum of 580 °C.

3.2.2. Anisotropy of magnetic susceptibility (AMS)

The AMS of a selection of sedimentary samples from all localities was measured to determine whether their magnetic fabrics have a mainly sedimentary or tectonic origin. In both cases, initial depositional compaction will impart an oblate magnetic fabric with the minimum axis K_3 perpendicular to the bedding due to compaction. In the case of a purely sedimentary fabric, the K_1 and K_2 axes are indistinguishable. Upon deformation, the maximum axis K_1 of the AMS tensor will gradually be directed parallel to the orientation of maximum extension or equivalently perpendicular to the orientation of maximum contraction resulting in distinctly separated K_1 and K_2 distributions in a tectonic fabric (Hrouda, 1982). In such cases, the geological context is crucial for determining whether the results indicate a pure extensional or compressional setting. When the statistical measurement errors are too high, all three axes will be indistinguishable; such results need to be discarded from further analysis and interpretation.

In this study, the AMS tensor was measured and calculated using an AGICO Kappabridge MFK1-FA (noise level 2.1 * 10^{-13} A m^2). Jelinek statistics (Jelinek, 1978, 1981) were used for the calculations of the AMS tensor. The resulting data were viewed and interpreted using AGICO Anisoft 4.2.

3.2.3. Vertical-axis rotations

Our samples were demagnetized stepwise in order to obtain their characteristic remanent magnetization (ChRM) vectors. For most samples, this was done using thermal demagnetization. Volcanic samples were heated stepwise with increasing temperature increments of 20–50 °C in an oven until they reached a temperature of 580 °C, while most sedimentary samples were heated until a temperature of about 420 °C. At these maximum temperatures, the samples were sufficiently demagnetized to determine the ChRM, while thermal alteration is minimized. In addition, some samples were demagnetized using

alternating field (AF) demagnetization. These samples were placed manually in a Helmholtz coil to provide a non-magnetic environment. Stepwise increasing alternating fields of 10 mT were applied in three directions for all samples until a field of 60 mT was reached. After each demagnetization step, the natural remanence magnetization (NRM) of the sample was measured on a 2G Enterprise horizontal cryogenic magnetometer equipped with three DC SQUIDS (noise level $3.0*10^{-12}$ Am^2) or an AGICO JR6 spinner magnetometer (noise level $2.5 * 10^{-11}$ Am^2).

For all paleomagnetic interpretations and subsequent statistics, the open-source and platform-independent portal "Paleomagnetism.org" was used (Koymans et al., 2016). The demagnetizations of all measured samples were plotted in orthogonal demagnetization plots (Zijderveld, 1967) for interpretation. Characteristic components were derived from this using principal component analysis (Kirschvink, 1980) or the great circle best-fit analysis (McFadden and McElhinny, 1988), while standard Fisher statistics (Fisher 1953) were used to calculate the means and corresponding dispersions (k, K) and cones of confidence (α95, A95) of the ChRM and virtual geomagnetic pole (VGP) distributions. Subsequently, errors in declination (ΔD_x) and inclination (ΔI_x) were calculated after Butler (1992). A 45° cut-off is applied to the ChRM/VGP distribution to determine which sites were used for constraining locality mean directions. Samples from tilted beds were corrected for their bedding plane. The A95 confidence envelope from Deenen et al. (2011, 2014) was used to determine whether a certain distribution represents paleosecular variation (PSV) or a spot reading. In the latter case, $A95 < A95_{min}$. In case $A95 > A95_{max}$, additional sources of scatter are present, such as small-scale rotational differences, chemical alteration, or measurement errors. The cartesian coordinate bootstrap test from Tauxe (2010) was used for determining whether two distributions from the same locality share a common true mean direction (CTMD). The fold test of Tauxe and Watson (1994) was utilized to check whether the magnetizations in a certain locality were acquired before or after tilting. Both tests were applied whenever possible.

4. Results

4.1. Paleomagnetism

4.1.1. Bulk magnetic susceptibility

The mass-normalized bulk magnetic susceptibility for four representative volcanic samples and two sedimentary samples from different localities is shown in Fig. 7 after seven consecutive heating and cooling cycles. Plots of intensity decay during thermal demagnetization are shown as well for comparison.

Andesitic sample AD06.3 shows a gradually increasing susceptibility up to 360 °C with only minor susceptibility changes during the first five heating cycles. These minor changes are likely related to chemical alteration due to oxidation. Between 360 °C and 420 °C, the susceptibility reaches a maximum. This maximum can be interpreted as a Hopkinson peak, which marks the transition from blocking temperatures to Curie temperatures for magnetic minerals in the sample (Hopkinson, 1989). The sharp susceptibility drop associated with the Curie temperature is observed at higher temperatures, and the susceptibility reaches a minimum at 580 °C, indicating that magnetite (Fe_3O_4) is the dominant magnetic carrier. However, the inflection of the curve towards a slighter decrease in susceptibility around 550 °C indicates that some Ti-poor titanomagnetite (Fe_2TiO_4) is involved, as the relative amount of titanium in magnetite leads to a gradual decrease in Curie temperature (Dunlop and Özdemir, 1997). The final cooling step is characterized by lower susceptibilities compared to the first heating cycles, implying that the sample underwent further oxidation. These observations correspond well to the intensity decay curve of AD06.3. This curve also shows a gradual decrease at first, followed by a faster decrease after 400 °C and a minimum intensity at 580 °C (Fig. 7).

The overall properties of a second andesitic sample, KD02.2, are generally the same as AD06.3, also displaying a sharp drop in susceptibility above 420 °C. However, the inflection related to the presence of Ti-poor titanomagnetite occurs at a lower temperature of around 530 °C in this sample, indicating a slightly larger amount of titanium. Furthermore, the Hopkinson peak is less clear. A maximum occurs around 300 °C, after which the susceptibility starts to decrease gradually. These observations could indicate the presence of maghemite or a higher degree of chemical alteration compared to AD06.3. The susceptibility curve of KD02.2 again corresponds nicely to its intensity decay curve (Fig. 7).

GL02.1 is a rhyolite sample, where (titano)magnetite is again the dominant magnetic carrier. However, the minimum susceptibility around 580 °C is substantially higher compared to AD06.3 and KD02.2. Furthermore, large susceptibility drops can be observed after each heating cycle beyond 360 °C. Both of these properties are an indication for the inversion of maghemite (γFe_2O_3) to hematite (Fe_2O_3), starting at 360 °C (Dankers, 1978). The presence of maghemite could be an indication for a high degree of weathering, related to low-temperature oxidation (Dunlop and Özdemir, 1997). This could have resulted in a partial overprint of the magnetization.

BY01.7 is basaltic in composition. It has a clearly defined Hopkinson peak at 360 °C. Its behavior after this peak is characteristic for the presence of Ti-poor titanomagnetite as the dominant magnetic carrier. This can also be clearly observed in the intensity decay curve, where a very sharp drop in intensity occurs at 400 °C (Fig. 7). Furthermore, the susceptibility values of BY01.7 are almost completely reversible after each cooling step, indicating a low amount of chemical alteration.

SV01.1 is a sedimentary specimen, composed of tuffite. It is characterized by low-intensity values, resulting in a noisy susceptibility curve. The maximum value is reached at 240 °C, after which the susceptibility gradually decreases during each subsequent heating step. The inflection of the curve towards faster susceptibility decrease can be observed at 360 °C (Fig. 7), indicating the occurrence of maghemite and its associated inversion.

The final sample IL04.9 is a greyish-white limestone from the lower sequence. It has a generally low magnetic susceptibility until temperatures higher than 400 °C are reached (Fig. 7). At this point, the susceptibility increases after each heating step. Such behavior is common for a sample containing pyrite (FeS_2). Pyrite is a paramagnetic mineral, but it oxidizes to ferromagnetic magnetite around 390–420 °C, resulting in an increase in susceptibility (Passier et al., 2001). Pyrite is a common mineral in organic-rich, oxygen-poor environments with a supply of iron. Therefore, its presence in IL04.9 is another indication that lower sequence limestones were formed in a fluvio-lacustrine environment. The formation of magnetite does not disturb the determination of the ChRM of IL04.9, because thermal demagnetization until 420 °C was sufficient to obtain a reliable direction, as evidenced by the intensity decay curve.

4.1.2. Anisotropy of magnetic susceptibility (AMS)

The AMS of selected samples from all sedimentary localities was measured. The measurement errors in samples from most localities were too high, resulting in undistinguishable fabrics for those localities. The large errors may be attributed to low overall intensities of the samples. Therefore, these localities were discarded. Only three localities (Evciler, Kapaklı, and Selvili) yielded results with low measurement errors, with a largely sedimentary fabric after bedding correction. The resulting AMS ellipsoids of these three localities are shown in Fig. 8, alongside their inferred extension directions. In all three cases, K_3 is oriented almost vertically, perpendicular to the bedding plane within its error margin. Furthermore, the K_1 and K_2 axes form a girdle perpendicular to the K_3-axis, resulting in an oblate AMS ellipsoid, as can also be seen from the shape parameter T (Fig. 8f).

AMS results of Evciler and Selvili show a tectonic fabric where K_1 and K_2 measurements form well-defined clusters (Fig. 8a and 8b). All three axes have a similar general orientation in both localities,

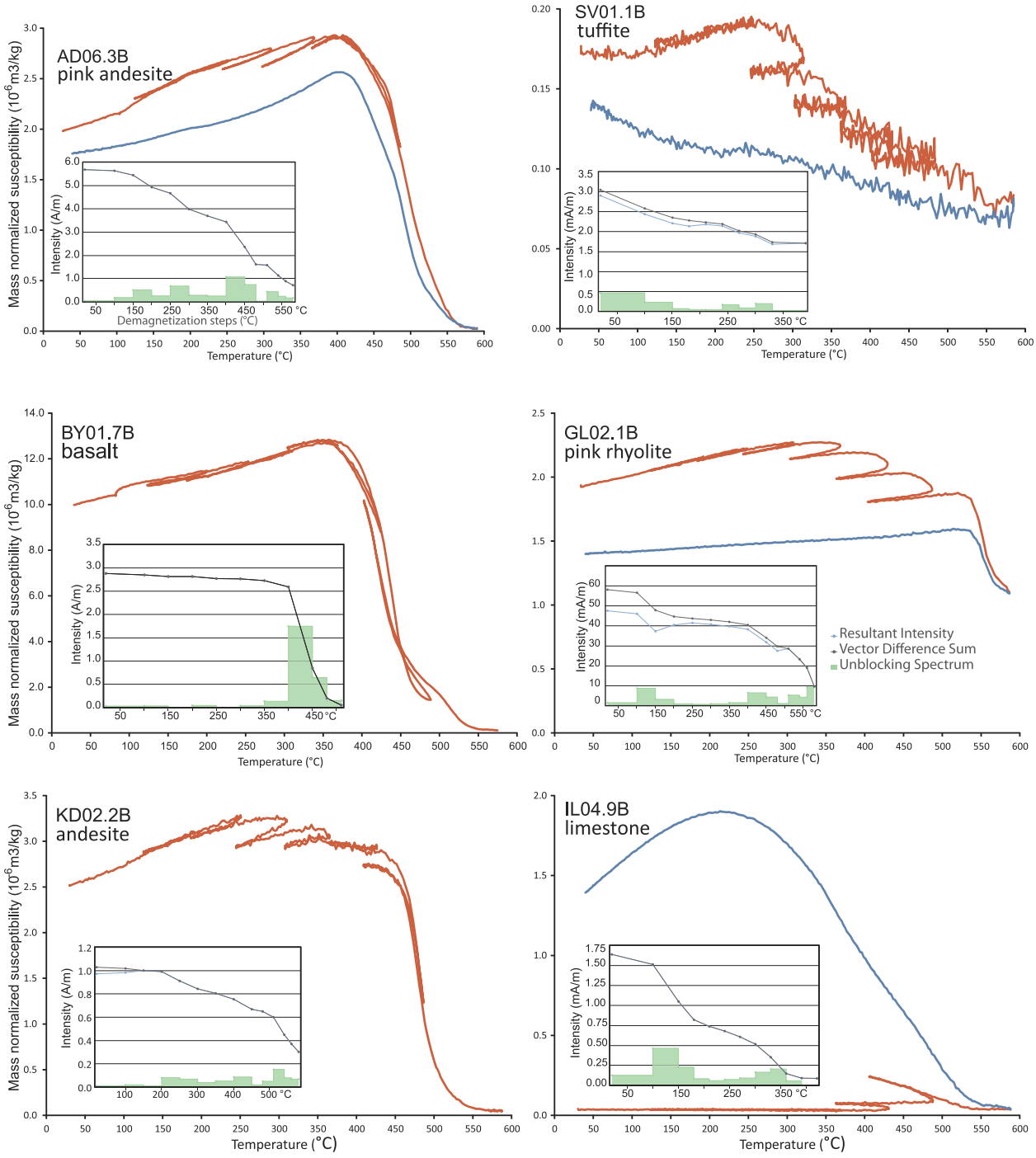

Fig. 7. Representative bulk magnetic susceptibility versus temperature curves during seven heating and cooling steps of 60 °C starting at 180 °C up to a maximum of 580 °C for 4 volcanic and 2 sedimentary samples. Bulk magnetic susceptibility is mass normalized (10^{-6} m^3/kg). Corresponding thermal demagnetization intensity decay plots are shown as well with: black line = vector difference sum, blue line = resultant intensity, green = unblocking spectrum.

indicating approximately N-S extension parallel to K_1 or, equivalently, perpendicular E-W trending contraction parallel to K2. The same orientations can be inferred from Kapaklı (Fig. 8c) even though the AMS axes show relatively poor clustering, although they still agree with the AMS results from Evciler and Selvili. Therefore, all results together (Fig. 8d) consistently indicate an approximately N-S extension and/or E-W contraction in the Soma basin during the deposition of the upper sequence. When comparing these results with the kinematic analyses (Fig. 5) and mapped structures (Figs. 2 and 4), we conclude that approximately N-S oriented extension took place along the İBTZ during the early Miocene.

4.1.3. Vertical-axis rotations

In total, 432 samples were demagnetized to obtain their ChRM directions. In many samples, a small viscous component is removed during the first few demagnetization steps. The mean paleomagnetic data for every measured site is listed per locality in Supplementary Table S1 in both a geographic and tectonic reference frame. The average declination D and its error ΔD_x from each locality were used to describe the vertical-axis rotations. Fig. 9 shows representative orthogonal demagnetization plots (Zijderveld, 1967) for both volcanic (Fig. 9a) and sedimentary samples (Fig. 9b). Example plots of white limestones from Beyoba (BO) and Kapaklı (KP) are indicated as well

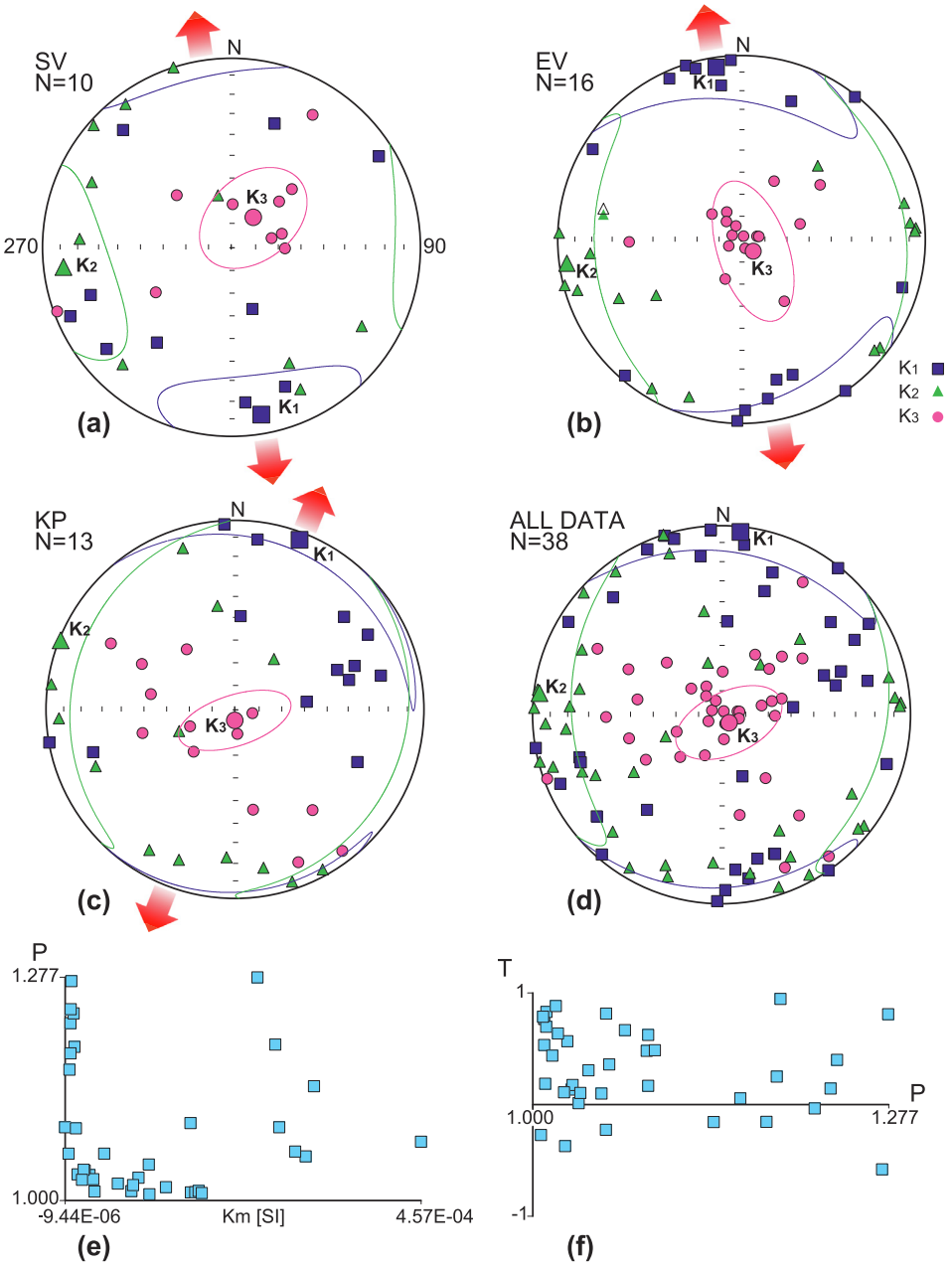

Fig. 8. Equal area projection of Anisotropy of Magnetic Susceptibility (AMS) results for three localities in the Soma basin in tectonic coordinates: (a) Evciler, (b) Selvili, (c) Kapaklı and (d) all data together; (e) anisotropy (P) versus bulk susceptibility, (f) shape diagram with shape parameter T (T > 0 is oblate, T < 0 is prolate), N = number of samples. Mean axes (large symbols) and corresponding confidence envelopes are shown. Resulting lineations (mean K1 axes) are indicated as red arrows. Lineations are parallel to extension directions.

(Fig. 9c). Unfortunately, these two lower sequence localities gave no results due to the low intensities of the samples; they were subsequently discarded. Magnetite is the dominant magnetic carrier in the majority of samples based on unblocking temperatures, but the demagnetization of sample GL03.2 suggests that a minority of samples could contain additional small occurrences of higher-coercivity components, such as hematite. Fig. 10 shows the equal-area projections of the ChRM directions and their means for all localities. We divide the localities into three separate blocks, according to their age and position in the basin (Fig. 2).

Kınık block: Göçbeyli (GB), Arpadere (AD), Karadere (KD), Kınık (KN) and Dereköy (DK) are all sampled localities from the south-western quadrant of the study area (Fig. 2) and together constitute the Kınık block (Fig. 10a). All localities are from the lower sequence of early Miocene age. The Göçbeyli location consists of nine volcanic sites (lava flows) from the lower sequence. Sites GB05 and GB06 both produced chaotic directions with low k values (4.2 and 5.8, respectively). Additionally, these sites were discarded by the 45° cut-off. The remaining sites produced a mean with a very shallow inclination (−7°) after tectonic correction. Therefore, the geographic reference frame gives a more consistent result for the Göçbeyli location (Table 1). Arpadere is part of the Yuntdağ volcanics (Fig. 3), and seven (andesitic) extrusions were sampled at this locality. It exhibits a well-determined CW rotation of 24 ± 10° in a geographic reference frame (Table 1, Fig. 10), and the only rejected site after applying a 45° cut-off is AD02 (Table S1). Karadere is another location in the Yuntdağ volcanics, consisting of nine volcanic (andesitic) sites. The locality shows a coherent CW rotation of 42 ± 10° (Fig. 10a, Table 1). Dereköy and Kınık

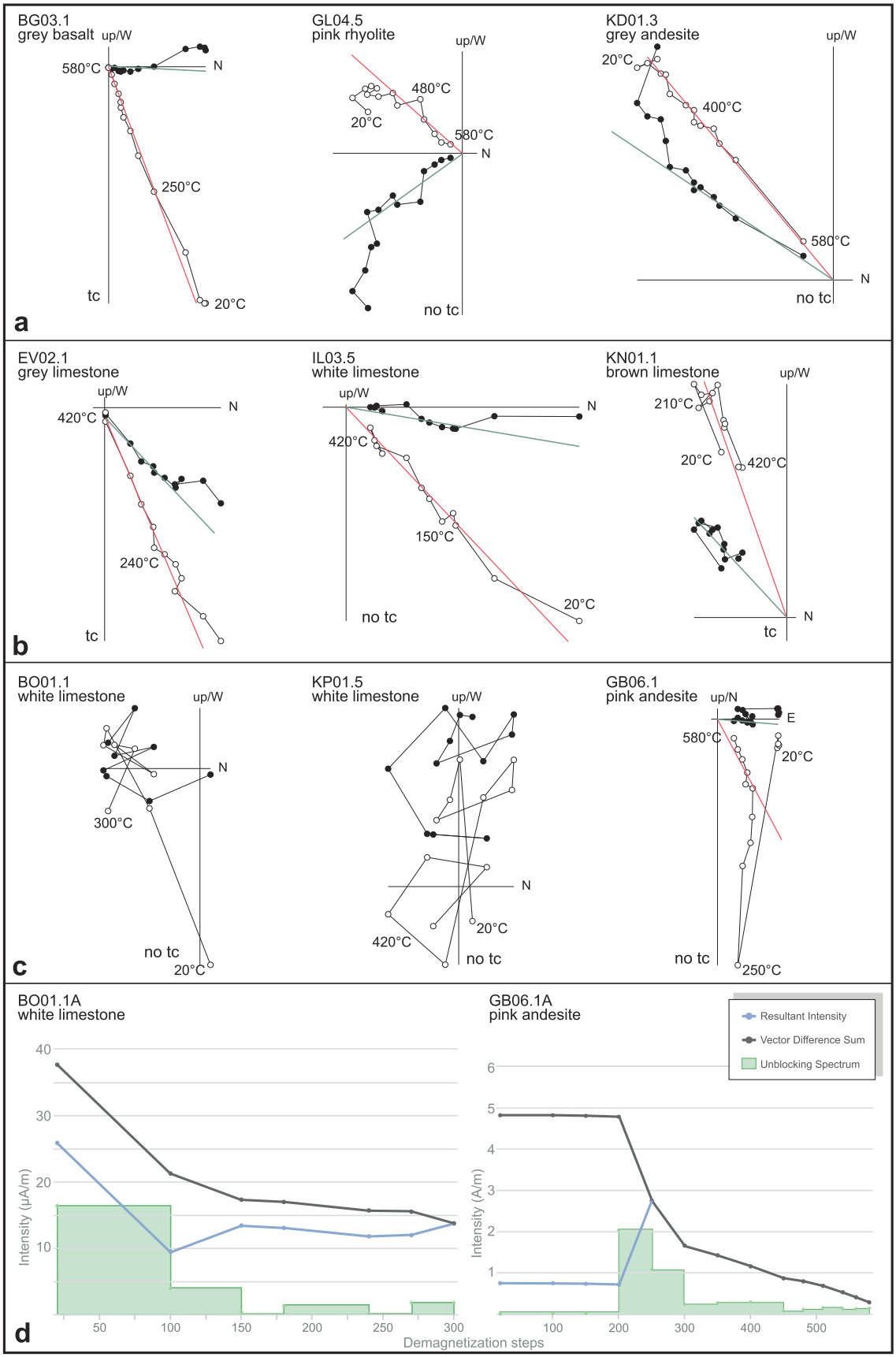

Fig. 9. Representative volcanic (a) and sedimentary (b) orthogonal vector diagrams (Zijderveld, 1967) from different lithologies in the study area. Open/closed circles indicate projections on the vertical/horizontal plane; tectonic (tilt corrected, tc) or geographic (no tc) reference frame is indicated, as well as thermal demagnetization steps. Vertical/horizontal projections of the characteristic components are shown in red/green. Some examples from rejected sites are shown (c) and two thermal demagnetization intensity decay diagrams (d).

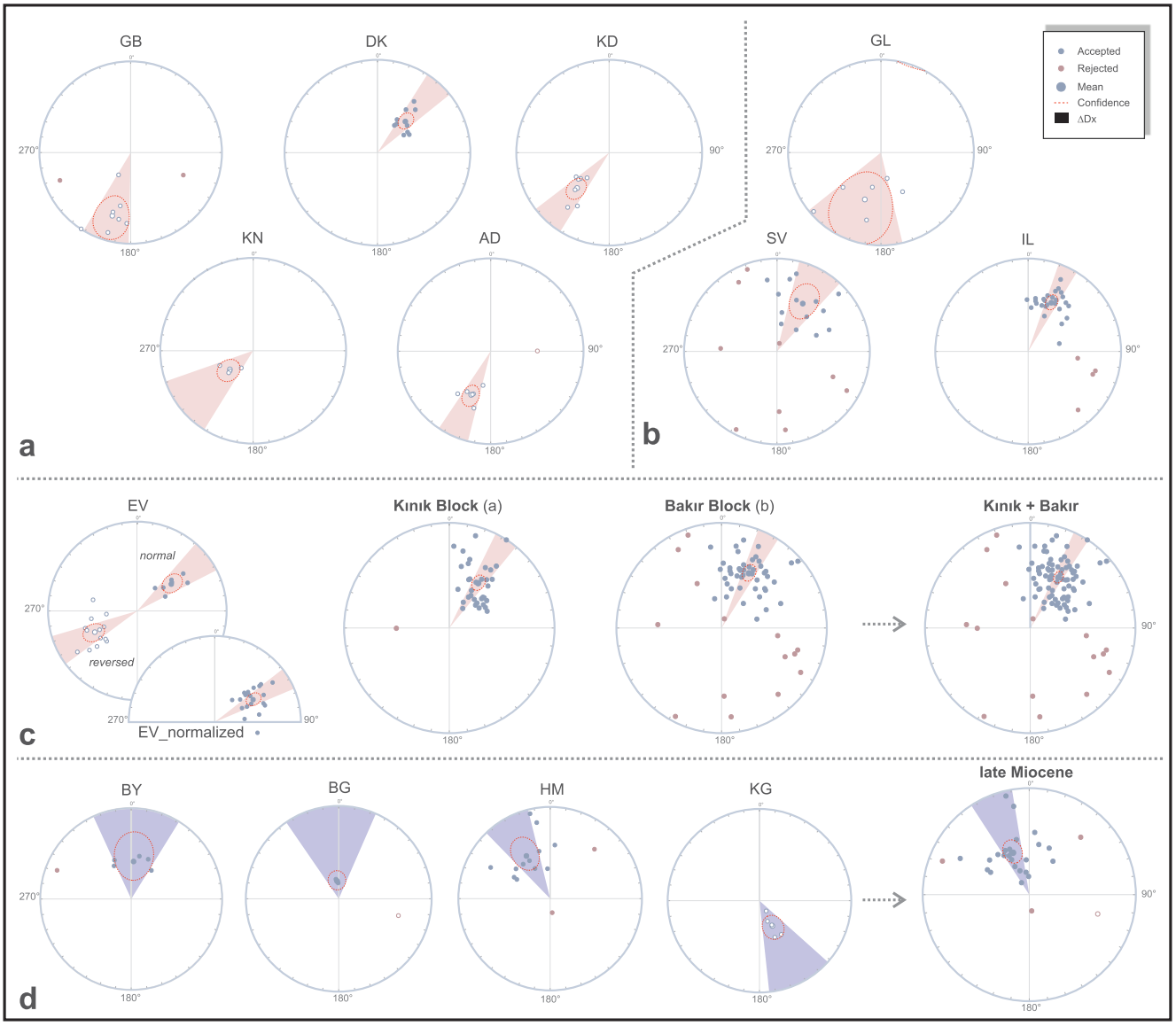

Fig. 10. Equal area projections of the ChRM directions for all sites. Sites have been grouped into (a) the Kınık block (SW Soma basin) and (b) the Bakır block (SE Soma Basin). In (c) we show the results of the Evciler (EV) locality and combine the results of the two blocks; (d) the middle-late Miocene sites and their compiled result showing a CCW rotation for the youngest rocks in the basin. Open/closed symbols indicate projection on upper/lower hemisphere. Blue/red circles denote accepted/rejected sites by the 45° cut-off. Mean directions (big blue circles) with their cone of confidence (red dashed line) and ΔD_x (light blue) are indicated as well. (No) tc = (not) tilt corrected. Locality abbreviations as in caption to Fig. 2.

are two sedimentary localities in the south-western quadrant of the study area (Fig. 2). KN01 is the only used site from the Kınık locality; the other three sites from this locality have very scattered directions ($A95 > A95_{max}$) and are therefore not used for the final result (Table S1). The average ΔD_x and A95 values from KN01 become slightly lower after tectonic correction. In addition, the tectonic correction resulted in a more consistent fit with the results from the previous three localities, producing a CW rotation of 51 ± 20° (Fig. 10a, Table 1). Dereköy produces a consistent CW rotation of 42 ± 9° after tectonic correction (Fig. 10a, Table 1). We applied the fold test on all localities from the Kınık block, but considering the large 95% confidence interval [3,94%] we consider it as indeterminate and hence inconclusive (Fig. S1a). Because the mean results from the Kınık block localities are similar and consistently do not plot in the present-day field even in a geographic reference frame, the fold test results are probably related to shortcomings of the fold test itself taking not into account the effect of non-horizontal deposition (paleo-topography) or noncoaxial differential tilting of the bedding planes alongside errors in bedding measurements of the thick volcanic flows making up the bulk of reliable results from the Kınık block (AD, KD, GC) rather than to post-folding magnetization. The final mean direction from the early Miocene sites of the Kınık block gives a CW rotation of 33 ± 7° (Fig. 10c, Table 1).

Bakır block: Selvili (SV), Ilyaslar (IL), and Gelembe (GL) are the three sampled localities in the south-eastern quadrant of the study area, separated from the south-western localities (Fig. 2), and together make up the Bakır block (Fig. 10b). İlyaslar consists of lower sequence fluvio-lacustrine and pyroclastic deposits. Selvili is similar to İlyaslar in terms of stratigraphic position (Figs. 2 and 3). It consists of two sites (SV1 and SV2), which form a NE-trending anticline. Before tilt correction, the two sites give more consistent directions implying that the magnetization has been acquired after tilting. Unfortunately, the results are too scattered to produce a reliable fold test for this locality, and many samples are rejected by the 45° cut-off (Fig. 10b, Table S1). Applying tilt correction results in a shallow inclination (25°) and a very low k value (7.6), indicating a high amount of scatter. In addition, the resulting rotation in geographic coordinates is consistent with İlyaslar.

Table 1
Mean paleomagnetic results from this study for the Bakır and Kınık blocks, and the combination of the two blocks forming the main results for the Soma basin. The results of locality EV and the late Miocene localities in the northern Soma basin are listed as well. All locality means are displayed in Fig. 10, while detailed paleomagnetic results are listed in Table S1. N = number of samples/sites after a fixed cut-off (45°), out of a total of Ns samples; D, I = mean declination, inclination; k, α_{95} / K, A95 = dispersion and 95% cone of confidence of the directional distribution / of the VGP distribution; ΔD_x, ΔI_x = the error in declination, inclination based on A95 of the VGP distribution (Butler, 1992); $A95_{min}$, $A95_{max}$ refers to the confidence envelope of Deenen et al. (2011, 2014) for sampling paleosecular variation.

Locality / Site		Formation	Lithology	N	Ns	D	ΔD_x	I	ΔI_x	k	α_{95}	K	$A95_{min}$ < A95 < $A95_{max}$
Kınık													
	Arpadere* (AD)	Yuntdağ volcanics	Rhyolite	6	7	24.1	9.9	47.4	10.3	67.2	8.2	60.7	5.9 < 8.7 < 26.5
	Göçbeyli* (GB)	Yuntdağ volcanics	Rhyolite, tuff	7	9	16.2	15.0	28.7	23.9	12.2	18.0	18.5	5.5 < 14.4 < 24.1
	Dereköy (DK)	Soma Formation	Sandstone, limestone, tuff	10	10	41.9	9.3	52.9	8.1	43.9	7.4	39.4	4.8 < 7.8 < 19.2
	Karadere (KD)	Yuntdağ volcanics	Rhyolite	7	7	42.2	10.4	47.3	10.8	35.7	10.2	44.9	5.5 < 9.1 < 24.1
	Kınık (KN)	Soma Formation	Sandstone, limestone	4	4	51.3	19.5	63.7	10.8	97.8	9.3	46.9	6.9 < 13.5 < 34.2
				34	**35**	**32.8**	**6.6**	**48.0**	**6.8**	**17.7**	**6.0**	**19.1**	**2.9 < 5.8 < 8.9**
Bakır													
	Gelenbe* (GL)	Yuntdağ volcanics	Rhyolite	6	6	19.0	32.4	45.6	35.2	6.5	28.5	6.5	$A95_{max}$ = 26.5 < 28.5
	İlyaslar* (IL)	Soma Formation	Limestone	26	30	25.4	6.2	41.5	7.6	30.3	5.2	26.2	3.3 < 5.6 < 10.5
	Selvili* (SV)	Soma Formation	Sandstone, limestone, tuff	14	23	28.3	14.4	41.1	17.8	10.4	12.9	10.1	4.2 < 13.2 < 15.6
				45	**59**	**26.5**	**6.0**	**41.5**	**7.4**	**16.6**	**5.4**	**15.8**	**2.6 < 5.5 < 7.5**
Kınık + Bakır				**79**	**94**	**29.0**	**4.5**	**44.3**	**5.1**	**16.6**	**4.0**	**16.5**	**2.1 < 4.0 < 5.2**
Late Miocene													
	Bağalan (BG)	Dededağ basalt	Basalt	2	3	354.6	29.0	74.5	8.3	947.1	8.1	336.6	9.1 < 13.7 < 53.0
	Bayat (BY)	Dededağ basalt	Basalt, limestone	5	6	3.6	28.2	56.0	21.6	24.8	15.7	12.7	6.3 < 22.3 < 29.7
	Küçükgüney (KG)	Deniş Formation	Siltstone	5	5	332.9	21.0	64.8	11.0	54.4	10.5	29.8	6.3 < 14.2 < 29.7
	Hamidiye (HM)	Dededağ basalt	Basalt, limestone, tuff	12	14	330.9	15.1	45.7	16.5	11.4	13.5	11.4	4.4 < 13.4 < 17.1
				24	**28**	**338.9**	**11.9**	**55.3**	**9.5**	**13.3**	**8.4**	**10.5**	**3.4 < 9.6 < 11.1**
Evciler (EV)													
	EV_nor	Soma Formation	Siltstone	7	7	51.9	11.0	49.6	10.6	39.8	9.7	41.9	5.5 < 9.4 < 24.1
	EV_rev	Soma Formation	Siltstone	13	13	243.5	10.1	−45.8	11.0	25.8	8.3	22.4	4.3 < 9.0 < 16.3
	EV_all			**20**	**20**	**59.6**	**7.6**	**47.3**	**8.0**	**28.5**	**6.2**	**24.8**	**3.6 < 6.7 < 12.4**

Gelembe consists of six horizontally deposited rhyolitic extrusions within the lower sequence. Gelembe is characterized by a degree of scatter in its mean declination with ΔD_x = 35° (Fig. 10b). Despite the scatter in these localities, the results are consistent when added together, producing a coherent mean direction for the Bakır block of 26.5 ± 6.0° in a geographic reference frame (Table 1) that is significantly different from a recent field direction. Indeed, the fold test for the Bakır block is negative (Fig. S1b), similar to the Kınık block. Therefore, this test result is most straightforwardly a consequence of the higher amount of scatter in the individual localities of the Bakır block.

Evciler site: Evciler consists mainly of grey organic-rich mudstones from the lower sequence of Miocene units (Fig. 3). It exhibits low scatter in both a geographic and tectonic reference frame. The inclination is too shallow (28°) in geographic coordinates but becomes steeper (47°) after tectonic correction (Table S1). The locality shows both normal and reversed polarities (Fig. 10), and the application of a bootstrap coordinate reversal test yields a positive result for Evciler (Fig. S2). Therefore, we can combine these paleomagnetic results leading to a considerable CW rotation of 60 ± 8° in tectonic coordinates. The age of the locality is mapped as early Miocene, but it is also close to some large faults. Therefore, we cannot confidently place this locality in any of the blocks above. However, the rotational phase derived from the Kınık block, Bakır block, and the Evciler locality falls into the middle Miocene age (Fig. 3).

Middle-late Miocene sites: Localities Bağalan (BG), Bayat (BY), Küçükgüney (KG) and Hamidiye (HM) are mostly located in the northern part of the study area (Fig. 2). Bağalan is a volcanic locality from the late Miocene Dededağ basalt (Fig. 3), consisting of three columnar basaltic sites. This locality yielded only two reliable sites since BG02 was rejected by the 45° cut-off (Fig. 10a, Table S1). The Bayat location consists of five volcanic and one sedimentary site derived from the upper sequence (Figs. 2 and 3). It provides no significant rotation (4 ± 28°), but the ΔD_x value is high, although it becomes less after tectonic correction (Table S1). BY06 is the only sedimentary site from the Bayat locality, but did not produce reliable results (k = 5.7, A95 > $A95_{max}$) and was additionally discarded by the 45° cut-off. Küçükgüney is a sedimentary locality within the upper sequence of the Soma basin, situated close to Evciler (Figs. 2 and 3). It produced only five reliable samples from one site, resulting in a CCW rotation of −27 ± 21° in tectonic coordinates (Fig. 10d, Table 1). The Hamidiye (HM) locality consists of five volcanic extrusions and one sedimentary site (HM03). HM06 produced an unrealistic direction (southward declination and downward-pointing inclination) and was subsequently rejected by the 45° cut-off. This resulted in a CCW rotation of −29 ± 15° in tectonic coordinates (Fig. 10d, Table S1). If we combine the results of all middle-late Miocene sites, we find a rotation of −21 ± 12° CCW as the youngest rotational phase.

All paleomagnetic data are listed in Table S1; the results per block or age interval are displayed in Table 1. We also provide the raw data as a Supplementary file (Data S1). Uzel et al. (2015) constrained average net rotations of 23 ± 6° CW (early Miocene, IBTZ) and −23 ± 10° CCW (early Miocene, Menderes region), while van Hinsbergen et al. (2010b) found an average 13 ± 9° CW rotation for Miocene rocks of the Northern Menderes Massif basins. All rotations mentioned here are with respect to the Eurasian Apparent Polar Wander Path (APWP) of Torsvik et al. (2012), where a declination of 3.5 ± 2.5° (10 Ma) up to 5.6 ± 2.5° (20 Ma) is expected at the current location of the Soma basin (Fig. S3).

5. Discussion

5.1. Spatio-temporal relationships

The İBTZ is interpreted as a large-scale NE-SW trending strike-slip shear zone in an extensional setting accommodating differential strain between the Menderes and Cycladic core complexes (Sözbilir et al., 2003; 2011; Uzel and Sözbilir, 2008; Uzel et al., 2013, 2015). The observed styles of structures within the İBTZ display a Riedel deformation pattern in map view (Fig. 11a and b). Therefore D1 dextral

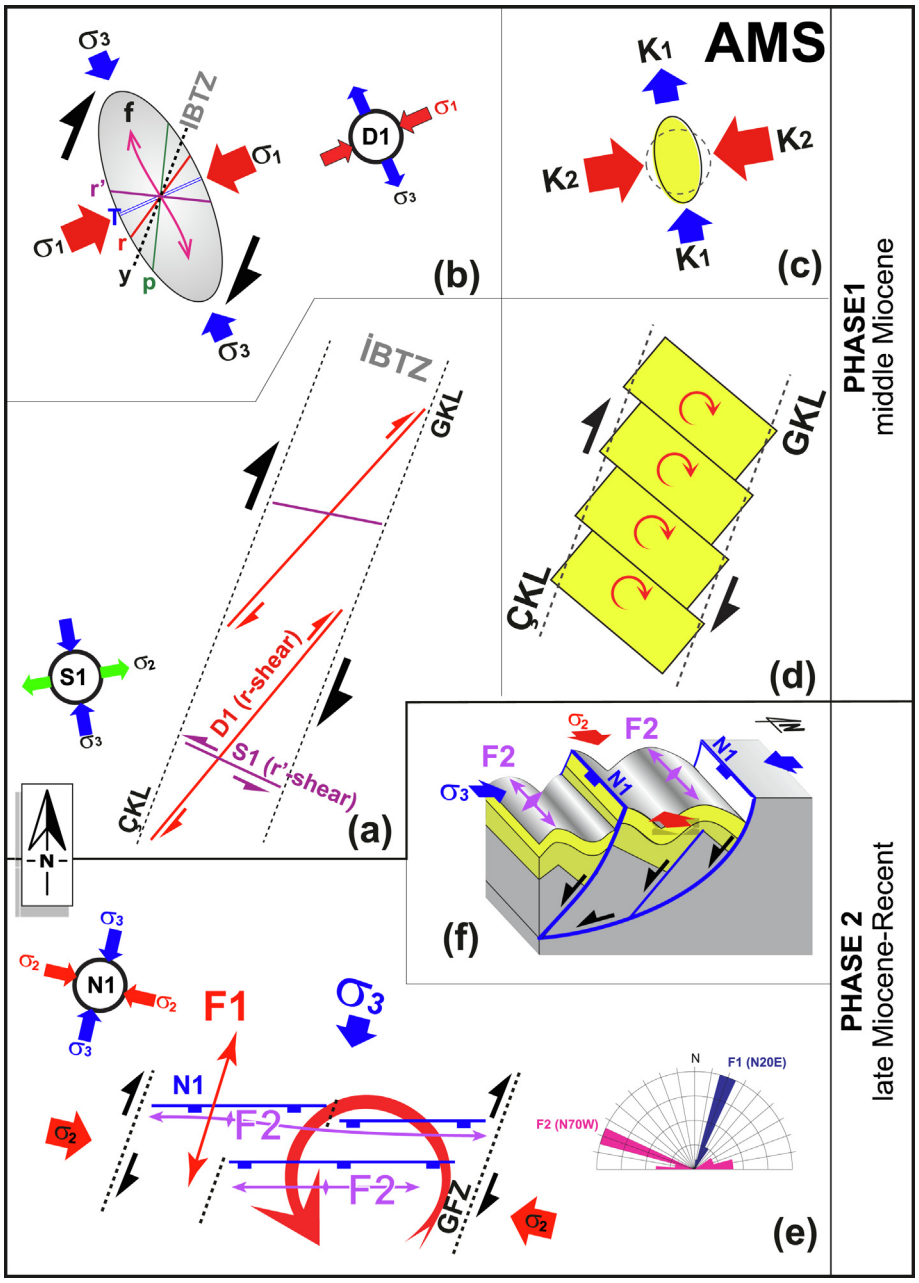

Fig. 11. (a) Schematic overview of early-middle Miocene deformation phase 1. GKL = Gelembe-Kemapaşa Lineament, ÇKL = Çandarli–Karaburun Lineament (Uzel et al., 2015), D1 and S1 refers to dextral and sinistral faults in Fig. 5. (b) Riedel Deformation ellipsoid (Dresen 1991). σ_1 and σ_3 are horizontal components of major and minor principal stresses. (c) Anisotropy of magnetic susceptibility (AMS) results, K_1 is lineation parallel to extension and K_2 is parallel to contraction (Note conformity of paleostress with these directions). (d) Schematic representation of tectonic block rotations as a result of dextral strike-slip faulting within the İBTZ during Phase 1. (e) Schematic representation of late Miocene-Pliocene deformation (Phase 2), which depicts normal faults (N1, Fig. 5) and associated folds (F2). Note that F2 folds are parallel to normal faults (N1) and are forced folds. (f) Block diagram depicting the geometric relationship between the forced folds, the normal faults and principal stress orientations.

strike-slip faults in the Soma basin correspond to the synthetic Riedel (R-) shears, while S1 sinistral strike-slip faults are the antithetic Riedel (R'-) shears based on their general orientations and field relationships. Both fault sets have normal oblique components, which is a common feature in strike-slip shear zones. This implies that both fault sets were developed simultaneously under NNW-SSE directed extension and related WSW-ENE trending compression (Figs. 5 and 10). The AMS results agree with this general configuration of the paleostress orientations, where the K1 axis is parallel to σ_3, and the K2 axis is parallel to the σ_1 direction (Fig. 11c).

We categorized the development of D1 and S1 faults as deformation Phase 1 and propose that it represents a transtensional deformation phase related to the initiation of the İBTZ as a wide dextral shear zone during the Miocene (Fig. 11a–d). This deformation style fits with other studies, such as NNW-SSE directed extension and NE-SW striking dextral strike-slip faulting in the southern part of the İBTZ around İzmir (Kaya, 1979; Erkül et al., 2005; Sözbilir et al., 2011; Uzel et al., 2013).

The E-W trending normal faults from fault set N1 cut and displace Phase 1 structures (Fig. 2), and also deformed the Pliocene Kumköy Formation. Most of the N1 normal faults have oblique-slip components, and they accommodate the development of folds. On the other hand, the NE-SW striking Gelembe Fault Zone, which is still active at present (Emre et al., 2013), is a dextral strike-slip fault (D1) that is contemporaneous with the activities of N1 faults. This suggests that these structures were developed under a new deformation regime, Phase 2, characterized by approximately N-S directed extension and E-W directed σ_2 related compression, while σ_1 is subvertical.

The F1 folds are not completely parallel to the expected folding direction of deformation phase 1 (compare "f" and "F1" in Fig. 11). These folds are mainly perpendicular to the σ_2 directions and parallel to σ_3 directions of deformation phase 2, implying that they are buckle folds developed in response to approximately WNW-ESE directed compression together with N1 faults (Fig. 11e). On the other hand, the E-W trending F2 folds are developed almost parallel to the nearby normal faults, and they are located mainly on the downthrown blocks of the normal faults (Fig. 11e–f). This relationship implies that these

folds are forced folds developed due to the bending of the cover rocks above normal fault blocks. Unlike F1 buckle folds – with fold axes perpendicular to the compression direction and parallel to the local extension direction (Fig. 11f) –, these forced folds develop in extensional settings (cf. Janecke et al., 1998) and their axes are perpendicular to the local extension direction. Çiftçi and Bozkurt (2009), Sözbilir (2002), and Uzel et al. (2013) found evidence for extensional folding along the Gediz Graben. The middle Miocene and younger rocks of the Soma basin are affected by F2 folding. Therefore, we propose that this folding must belong to Phase 2, contemporaneous with N1 normal faults. Although both deformation Phases 1 and 2 are of transtensional nature, field and age relationships show that extensional deformation became more dominant during the second phase and is currently still active.

5.2. Rotational phases

The paleomagnetic results of this study acquired in the early Miocene localities show an average net rotation of 33 ± 7° CW for the Kınık block and 26.5 ± 6° CW for the Bakır block. The rotation of the Bakır block is slightly less (~6°) CW than that of the Kınık block. The directions of the two blocks do not share a CTMD according to the coordinate bootstrap test, but their errors in declination overlap. After combining the results of the two blocks, we arrive at an average rotation of 29 ± 5° for the south-central Soma basin (Table 1). It seems that the ChRMs of both blocks have possibly been acquired during strike-slip faulting along the İBTZ, and the difference in rotation (~6°) between them may reflect a differential CW rotation through time. This would also provide an additional explanation for the inconclusive and negative fold tests from the Kınık and Bakır blocks, alongside the potential influence of paleo-topography and uncertainties in tilt correction on the fold tests, as discussed above (Section 4.1.3), implying that magnetic acquisition was contemporaneous with folding in an actively deforming region. In any case, the results imply that the first rotational stage of the Soma basin took place within a dextral shear zone, which is also evidenced by the coeval development of the Riedel deformation pattern within the İBTZ during the middle Miocene (Phase 1, Fig. 11). Furthermore, the paleomagnetic results from this study are in good agreement with previous paleomagnetic results obtained from the İBTZ. Uzel et al. (2015) reported an average net CW rotation of 23 ± 6° from the Yuntdağ region, while the Söke basin in the southern part of the İBTZ also has a rotation of 23 ± 6° CW (Uzel et al., 2017). These rotations are in good agreement with the rotation of the Bakır block in this study and have the same sense (CW) of rotation as those from the Kınık block, although the latter shows a significant larger CW rotation by ~10°, which may be an augmented rotation caused by local rotation of smaller blocks caught within the large shear zone. Indeed, the rotations within the Kınık block vary between 16° and 51° (Table 1), which indicates internal deformation of the block. We note that the rotations within the Yuntdağ region vary as well, between 16° and 33° (Uzel et al., 2015).

The second rotational phase in the İBTZ is shown by a −22 ± 11° CCW rotation from middle-late Miocene rocks (Fig. 12), which took place since the late Miocene (Uzel et al., 2015). In this study, we find a −21 ± 12° CCW rotation from the late Miocene rocks in the Soma basin, identical to the İBTZ rotations (Uzel et al., 2015). Therefore, we suggest the early Miocene rocks of Soma basin experienced a significant CW rotation (~50° in total) in the middle Miocene, which is almost similar in sense and magnitude (~45° CW) as found in the central sector of İBTZ (Uzel et al., 2015). Hence, we conclude that the Soma basin has experienced the same rotational history as the other Miocene basins along the İBTZ, while it was different from the Miocene basins on top of the MCC (van Hinsbergen et al., 2010b; Uzel et al., 2015; Kaymakcı et al., 2018).

5.3. Regional implications

The structural and paleomagnetic results from this study indicate that the study area experienced at least two co-axial deformation phases, both characterized by approximately E-W compression and N-S extension, which is also supported by AMS results (Figs. 8 and 11c). Both phases are characterized by transcurrent tectonics dominated by transtensional deformation with the role of extensional deformation becoming prominent in the second deformation phase. The observations from this and our earlier studies indicate that the İBTZ evolved from a wide shear zone (Phase 1) into narrow strike-slip fault zones, such as the Kaleköy (Özkaymak et al., 2013) and the Gelembe Fault Zones (Emre et al., 2016), where normal and strike-slip faults were effectively decoupled and extensional deformation progressively dominated in the region (Phase 2). The middle-late Miocene basaltic volcanic centers of the upper sequence have a clear NE-trend along these localized strike-slip faults (Fig. 2). Uzel et al. (2013, 2015) proposed a similar evolutionary model for the southern parts of the İBTZ, which they related to strain softening that was possibly facilitated by heat from the Miocene magmatism. This implies that the İBTZ extended northwards during the early Miocene into our study area (Fig. 12). In addition, we also point out that the southern branches of the North Anatolian Fault Zone (Sözbilir et al., 2017; Sümer et al., 2018) could have influenced the CCW rotation during the second rotational phase of Soma Basin. We speculate that the North Anatolian Fault Zone may have acted as a block boundary structure in the north since the late Miocene, but this requires additional research.

The two transtensional deformation phases proposed in this and previous studies (e.g., Brun, 1999; Brun et al., 2016; Schueller et al., 2005, 2010; Uzel et al., 2017) agree excellently with the (at least) two-stage Neogene trans(ex-)tension hypothesis for the whole Aegean region. This scenario suggests that a distinct transition from localized to distributed extension occurred in the middle Miocene, which could have been caused by an increase in strain rate. Brun et al. (2016) related this increase to the acceleration of roll-back of the Aegean slab, and it seems that this acceleration is responsible for differentiation in the rotational behavior of the western Anatolian-Aegean upper continental crust (Uzel et al., 2017).

6. Conclusions

New structural, AMS, and paleomagnetic data from the Soma basin show that it evolved as a strike-slip basin as a part of the İBTZ since at least the Neogene. According to our structural and AMS results, deformation was dominated by NE-SW trending dextral strike-slip faulting related to approximately N-S trending extension during two deformation phases. Early Miocene localities show CW rotations of on average 29 ± 5°, ranging from 33 ± 7° (Kınık block) to 27 ± 6° (Bakır block), while late Miocene localities show a a rotation of −21 ± 12° CCW. This indicates that the Soma basin was part of a large-scale dextral shear zone and underwent a ~50° CW rotation during the middle Miocene deformation (Phase 1). In the subsequent late Miocene to recent deformation phase (Phase 2), the distribution of NE-SW trending dextral strike-slip faulting narrowed and decoupled from the formation of E-W trending normal faults, while the Soma basin underwent an around −21° CCW rotation. It seems that this rotation is compensated mainly by distinct strike-slip faults such as the Kaleköy, Gelembe, and Havran-Balıkesir Fault Zones since the late Miocene. Our results are in excellent agreement with the rest of the İBTZ, indicating that it continues northward up until at least the northern part of the Soma basin.

In this context, the results from this and earlier studies show that the İBTZ effectively accommodated asymmetric extensional exhumation of the MCC and possibly the CCC during the middle Miocene deformation phase, after which the mode of extension changed from localized to distributed extension, related to the tearing of the northwards

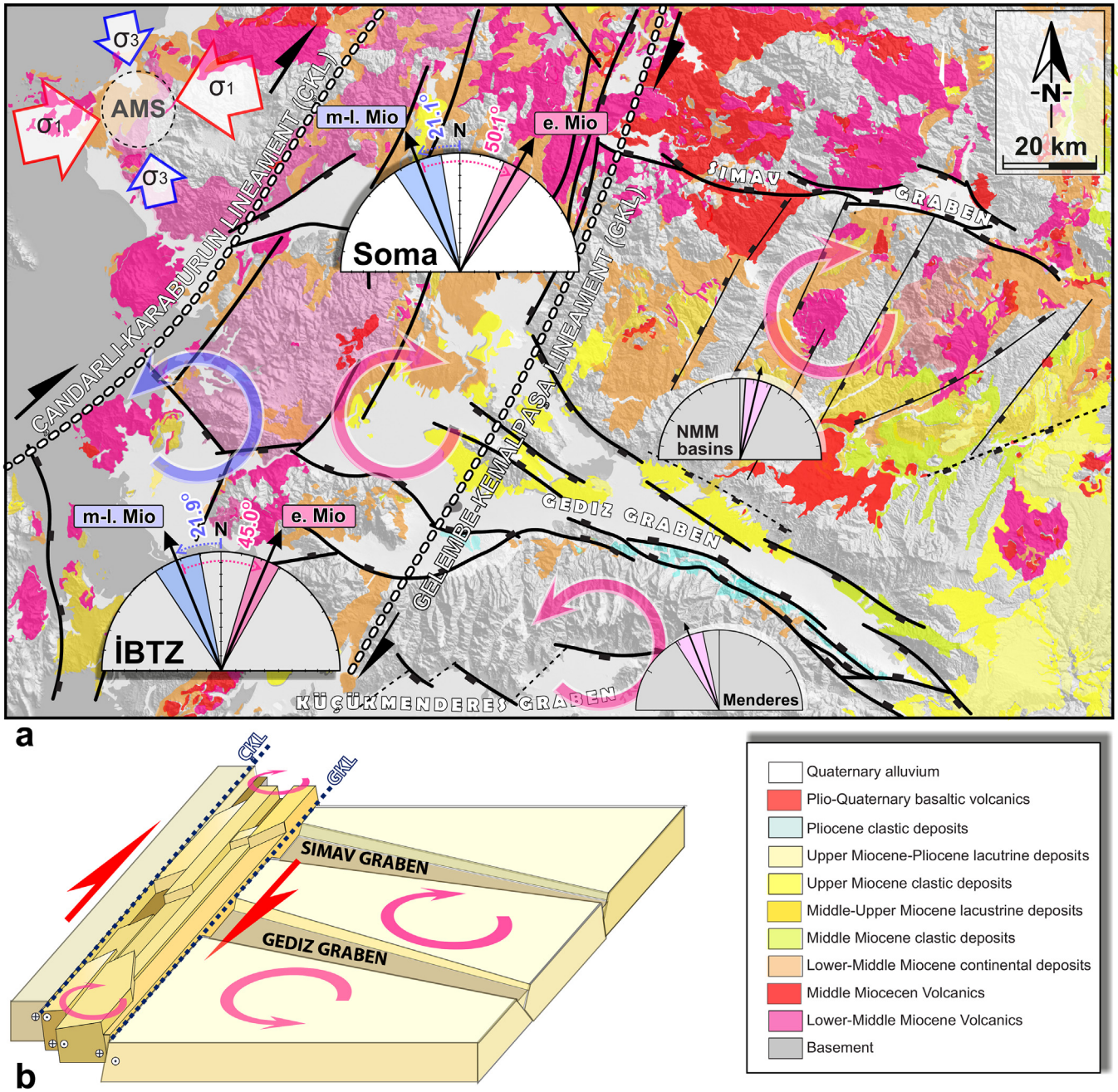

Fig. 12. Schematic representation of western Anatolian rotational phases since the Miocene (after Özkaymak et al., 2013; Uzel et al., 2013 and references therein). (a) Rotation of different tectonic blocks are drawn using the results from van Hinsbergen et al. (2010b) for the Northern Menderes Massif (NMM) basins, from Uzel et al. (2015) for the IBTZ and the Menderes massif, and the results of this study (Kınık, Bakır and late Miocene); pink (blue) shading refers to early (late) Miocene paleomagnetic results. Note that the Gediz Graben separates domains with CW rotation in the northern Menderes region from CCW rotation in the southern Menderes region. Paleostress directions σ_1 and σ_3 are indicated with red and blue arrows, respectively. Black lines with boxes (on the hanging-wall block) are normal faults. The recently active faults are thicker. (b) Simplified tectonic block model of the first deformational phase and its rotation senses.

subducting African oceanic slab below the western Anatolian - Aegean region (overriding plate) and subsequent acceleration of roll-back. The response of the overriding plate was segmentation into small structural blocks with differential rotation, delimited by approximately NE-SW strike-slip and E-W normal faults. The results also imply a possible link between the İBTZ and North Anatolian Fault Zone (NAFZ), at least since the late Miocene, inviting further investigation of the region.

CRediT authorship contribution statement

Jan Westerweel: Investigation, Data curation, Formal analysis, Writing - original draft. **Bora Uzel:** Investigation, Conceptualization, Methodology, Writing - review & editing. **Cornelis G. Langereis:** Investigation, Supervision, Methodology, Software. **Nuretdin Kaymakci:** Investigation, Supervision, Conceptualization, Writing - review & editing. **Hasan Sözbilir:** Supervision, Validation.

Declaration of Competing Interest

The authors declare that they have no known competing financial interests or personal relationships that could have appeared to influence the work reported in this paper.

Acknowledgments

We thank Emre Kırhan, İsmail Duran, Elif Çakır and İrem Avcu from the Dokuz Eylül University for their assistance during the paleomagnetic sampling, structural mapping and drawing figures. In addition, we thank Lennart de Groot, Annique van der Boon, Dan Palcu, Maxim Krasnoperov, and Annemarieke Béguin from the Fort Hoofddijk Paleomagnetic Laboratory for their advice and assistance during the paleomagnetic experiments. Finally, we are grateful to Laura Gregory, Marco Maffione, Assoc.Editor Ibrahim Uysal and two anonymous reviewers for their constructive suggestions and comments. This work is supported by the Scientific and Technical Research Council of Turkey (TÜBİTAK) research grant of ÇAYDAĞ-117R011.

Appendix A. Supplementary material

Supplementary data to this article can be found online at https://doi.org/10.1016/j.jseaes.2020.104305.

References

Akkök, R., 1983. Structural and metamorphic evolution of the Menderes Massif: new data from the Derbent area and their implication for the tectonics of the massif. J. Geol. 91, 342–350.
Aktuğ, B., Kılıçoğlu, A., 2006. Recent crustal deformation of İzmir, western Anatolia and surrounding regions as deduced from repeated GPS measurements and strain field. J. Geodyn. 41, 471–484.
Aldanmaz, E., Pearce, J.A., Thirlwall, M.F., Mitchell, J.G., 2000. Petrogenetic evolution of late Cenozoic, post-collision volcanism in western Anatolia, Turkey. J. Volcanol. Geoth. Res. 102 (1), 67–95.
Altunkaynak, Ş., Rogers, N.W., Kelley, S.P., 2010. Causes and effects of geochemical variations in late Cenozoic volcanism of the Foça volcanic centre, NW Anatolia, Turkey. Int. Geol. Rev. 52 (4–6), 579–607.
Arpaliyiğit, İ., 2004. Pliocene-Quaternary geology of the Soma graben, western Turkey. (PhD-thesis submitted to Graduate School of Natural and Applied Sciences of Dokuz Eylül University). Dokuz Eylül University, İzmir, Turkey.
Beccaletto, L., Steiner, C., 2005. Evidence of two-stage extensional tectonics from the northern edge of the Edremit Graben, NW Turkey. Geodinamica Acta 18 (3–4), 283–297.
Biryol, C.B., Beck, S.L., Zandt, G., Özacar, A.A., 2011. Segmented African lithosphere beneath the Anatolian region inferred from teleseismic P-wave tomography. Geophys. J. Int. 184 (3), 1037–1057.
Bozkurt, E., Park, R.G., 1997. Microstructures of deformed grains in the augen gneisses of southern Menderes massif and their tectonic significance, western Turkey. Geol. Rundsch. 86, 101–119.
Bozkurt, E., 2000. Timing of extension on the Büyük Menderes Graben, western Turkey, and its tectonic implications, in Tectonics and Magmatism in Turkey and the Surrounding Area, E. Bozkurt et al. (Eds.). Geol. Soc. Spec. Publ., 173, 385–403, 10.1144/GSL.SP.2000.173.01.18.
Borsi, J., Ferrara, G., Innocenti, F., Mazzuoli, R., 1972. Geochronology and petrology of recent volcanics in the eastern Aegean Sea (West Anatolia and Lesvos Iceland). Bull. Volcanol. 36, 473–496.
Bozkurt, E., 2001. Neotectonics of Turkey—a synthesis. Geodin. Acta 14, 3–30.
Bozkurt, E., 2003. Origin of NE-trending basins in western Turkey. Geodin. Acta 16 (2–6), 61–81.
Bozkurt, E., Sözbilir, H., 2004. Tectonic evolution of the Gediz Graben: field evidence for an episodic, two extension in western Turkey. Geol. Mag. 141, 63–79.
Bozkurt, E., Mittwede, S.K., 2005. Introduction: evolution of Neogene extensional tectonics of western Turkey. Geodin. Acta 18, 153–165.
Bozkurt, E., Rojay, B., 2005. Episodic, two-stage Neogene extension and short-term intervening compression in Western Turkey: field evidence from the Kiraz Basin and Bozdağ Horst. Geodin. Acta 18 (3–4), 299–316.
Bozkurt, E., Sözbilir, H., 2006. Evolution of the large-scale active Manisa Fault, southwest Turkey: implications on fault development and regional tectonics. Geodin. Acta 19, 427–453.
Brun, J.P., 1999. Narrow rifts versus wide rifts: inferences for the mechanics of rifting from laboratory experiments. Philos. Trans. –Roy. Soc. Lond. A Math. Phys. Eng. Sci. 695–709.
Brun, J., Faccenna, C., Gueydan, F., Sokoutis, D., Philippon, M., Kydonakis, K., Gorini, C., 2016. The two-stage Aegean extension, from localized to distributed, a result of slab rollback acceleration. Can. J. Earth Sci cjes-2015-0203.R1.
Butler, R.F., 1992. Paleomagnetism: Magnetic Domains to Geologic Terranes. Black-well Publishing, Boston, pp. 195.
Candan, O., Dora, O.Ö., Oberhansli, R., Oelsner, F., Durr, S., 1997. Blueschist relics in the Mesozoic cover series of the Menderes Massif and correlations with Samos Island, Cyclades. Schweiz. Mineral. Petrogr. Mitt. 77, 95–99.
Candan, O., Dora, O.Ö., Oberhansli, R., Çetinkaplan, M., Partzsch, J.H., Warkus, F.C., Durr, S., 2001. Pan-African high-pressure metamorphism in the Precambrian basement of the Menderes Massif, Western Anatolia, Turkey. Int. J. Earth Sci. 89, 793–811.
Christie-Blick, N., Biddle, K.T., 1985. Deformation and basin formation along strike-slip faults. In: Biddle, K.T and Christie-Blick, N. (Eds.) Strike Slip Deformation, Basin Formation and Sedimentation. SEPM Special Publication No.37. Tulsa, Oklahoma.
Çiftçi, N.B., Bozkurt, E., 2009. Evolution of the Miocene sedimentary fill of the Gediz Graben, SW Turkey. Sedimentary Geol. 216, 49–79. https://doi.org/10.1016/j.sedgeo.2009.01.004.
Dankers, P.H.M., 1978. Magnetic properties of dispersed natural iron-oxides of known grain size. ISO 690.
Deenen, M.H.L., Langereis, C.G., van Hinsbergen, D.J.J., Biggin, A.J., 2011. Geomagnetic secular variation and the statistics of palaeomagnetic directions. Geophys. J. Int. 186, 509–520.
Deenen, M.H.L., Langereis, C.G., van Hinsbergen, D.J.J., Biggin, A.J., 2014. Erratum to: Geomagnetic secular variation and the statistics of palaeomagnetic directions [Geophys. J. Int. 186 (2011) 509–520]. Geophys. J. Int. 197, 643.
Delvaux, D., Sperner, B., 2003. New aspects of tectonic stress inversion with reference to the TENSOR program. Geol. Soc. Lond., Special Publications 212 (1), 75–100.
Dewey, J.F., Hempton, M.R., Kidd, W.S.F., Şaroğlu, F., Şengör, A.M.C., 1986. Shortening of continental lithosphere: the neotectonics of eastern anatolia-a young collision zone. Geol. Soc. Spec. Pub. 19, 3–37.
Dunlop, D.J., Özdemir, Ö., 1997. Rock Magnetism – Fundamentals and Frontiers.
Ercan, E., Satır, M., Sevin, D., Türkecan, A., 1996. Batı Anadolu'daki Tersiyer ve Kuvaterner yaşlı volkanik kayaçlarda yeni yapılan radyometrik yaş ölçümlerinin yorumu [Some new radiometric ages from Tertiary and Quaternary volcanic rocks from West Anatolia]. Miner. Res. Explor. Bull. (Turkey) 119, 103–112.
Emre, Ö., Duman, T.Y., Özalp, S., Şaroğlu, F., Olgun, Ş., Elmacı, H., Çan, T., 2016. Active fault database of Turkey. Bull. Earthq. Eng. 1–47. https://doi.org/10.1007/s10518-016-0041-2.
Emre, T., Sözbilir, H., 2007. Tectonic evolution of the Kiraz Basin, Küçük Menderes Graben: evidence for compression/uplift-related basin formation overprinted by extensional tectonics in West Anatolia. Turk. J. Earth Sci. 16 (4), 441–470.
Erdoğan, B., 1990. Tectonic relations between İzmir-Ankara Zone and Karaburun Belt. Bull. Miner. Res. Explor. Inst. Turkey 110, 1–15.
Erkül, F., Helvacı, C., Sözbilir, H., 2005. Stratigraphy and geochronology of the Early Miocene volcanic units in the Bigadiç Borate Basin, Western Turkey. Turk. J. Earth Sci. 14, 227–253.
Erkül, F., Erkül, S.T., Ersoy, Y., Uysal, İ., Klötzli, U., 2013. Petrology, mineral chemistry and Sr–Nd–Pb isotopic compositions of granitoids in the central Menderes metamorphic core complex: constraints on the evolution of Aegean lithosphere slab. Lithos 180, 74–91.
Ersoy, Y.E., Helvacı, C., Uysal, İ., Karaoğlu, Ö., Palmer, M.R., Dindi, F., 2012a. Petrogenesis of the Miocene volcanism along the İzmir-Balıkesir Transfer Zone in western Anatolia, Turkey: implications for origin and evolution of potassic volcanism in post-collisional areas. J. Volcanol. Geoth. Res. 241, 21–38.
Ersoy, E.Y., Dindi, F., Karaoglu, Ö., Helvacı, C., 2012b. Soma Havzası ve Çevresindeki Miyosen Volkanizmasının Petrografik ve Jeokimyasal Özellikleri. Yerbilimleri 33, 59–80.
Fisher, R.A., 1953. Dispersion on a sphere. Proceedings of the Royal Society of London, Series A, 217, 295–305, 10.1098/rspa.1953.0064.
Forster, M., Lister, G., 2009. Core-complex-related extension of the Aegean lithosphere initiated at the Eocene-Oligocene transition. J. Geophys. Res. Solid Earth 114 (B2).
Gautier, P., Brun, J.P., Moriceau, R., Sokoutis, D., Martinod, J., Jolivet, L., 1999. Timing, kinematics and cause of Aegean extension: a scenario based on a comparison with simple analogue experiments. Tectonophysics 315 (1), 31–72.
Genç, C.Ş., Altunkaynak, Ş., Karacık, Z., Yazman, M., Yılmaz, Y., 2001. The Çubukludağ graben, south of İzmir: its tectonic significance in the Neogene geological evolution of the western Anatolia. Geodin. Acta 14 (1–3), 45–55.
Gessner, K., Gallardo, L.A., Markwitz, V., Ring, U., Thomson, S.N., 2013. What caused the denudation of the Menderes Massif: review of crustal evolution, lithosphere structure, and dynamic topography in southwest Turkey. Gondwana Res. 24 (1), 243–274.
Glodny, J., Hetzel, R., 2007. Precise U-Pb ages of syn-extensional Miocene intrusions in the central Menderes Massif, western Turkey. Geol. Mag. 144 (02), 235–246.
Govers, R., Wortel, M.J.R., 2005. Lithosphere tearing at STEP faults: response to edges of subduction zones. Earth Planet. Sci. Lett. 236 (1), 505–523.
Hopkinson, J., 1989. Magnetic and other physical properties of iron at a high temperature. Philos. Trans. Roy. Soc. Lond. A 180, 443–465.
Hrouda, F., 1982. Magnetic anisotropy of rocks and its application in geology and geophysics. Geophys. Surv. 5 (1), 37–82.
İnan, S., Pabuçcu, Z., Kulak, F., Ergintav, S., Tatar, O., Altunel, E., Saatçılar, R., 2012. Microplate boundaries as obstacles to pre-earthquake strain transfer in Western Turkey: inferences from continuous geochemical monitoring. J. Asian Earth Sci. 48, 56–71.
İnci, U., 1998. Lignite and carbonate deposition in Middle Lignite succession of the Soma Formation, Soma coalfield, western Turkey. Int. J. Coal Geol. 37 (3), 287–313.
İnci, U., 2002. Depositional evolution of Miocene coal successions in the Soma coalfield, western Turkey. Int. J. Coal Geol. 51, 1–29.
Janecke, S.U., Vandenburg, C.J., Blankenau, J.J., 1998. Geometry, mechanisms and significance of extensional folds from examples in the Rocky Mountain Basin and Range province, USA. J. Struct. Geol. 20 (7), 841–856.
Jelinek, V., Kropáček, R.V., 1978. Statistical processing of anisotropy of magnetic susceptibility measured on groups of specimens. Stud. Geophys. Geod. 22 (1), 50–62.
Jelinek, V., 1981. Characterization of the magnetic fabric of rocks. Tectonophysics 79 (3–4), T63–T67.
Jolivet, L., Brun, J.P., 2010. Cenozoic geodynamic evolution of the Aegean. Int. J. Earth Sci. 99, 109–138.
Jolivet, L., Faccenna, C., Huet, B., Labrousse, L., Le Pourhiet, L., Lacombe, O., et al., 2013.

Aegean tectonics: strain localisation, slab tearing and trench retreat. Tectonophysics 597, 1–33.
Karacık, Z., Genç, Ş.C., Gülmez, F., 2013. Petrochemical features of Miocene volcanism around the Çubukludağ graben and Karaburun peninsula, western Turkey: implications for crustal melting related silicic volcanism. J. Asian Earth Sci. 73, 199–217.
Kaya, O., 1979. Ortadoğu Ege çöküntüsünün (Neojen) stratigrafi si ve tektoniği [Neogene Stratigraphy and tectonics of the middleeast Aegean depression]. Geol. Soc. Turk. Bull. 22, 35–58 [in Turkish with English abstract].
Kaya, O., 1981. Miocene reference section for the coastal parts of West Anatolia. Newsl. Stratigr. 10, 164–191.
Kaya, O., Ünay, E., Saraç, G., Eichhorn, S., Hassenrück, S., Knappe, A., Pekdeğer, A., Mayda, S., 2004. Halitpaşa transpressive zone: implications for an Early Pliocene compressional phase in central western Anatolia, Turkey. Turkish J. Earth Sci. 13 (1), 1–13.
Kaya, O., Ünay, E., Göktaş, F., Saraç, G., 2007. Early Miocene stratigraphy of central west Anatolia, Turkey: implications for the tectonic evolution of the eastern Aegean area. Geol. J. 42, 85–109. https://doi.org/10.1002/gj.1071.
Kaymakci, N., 2006. Kinematic development and paleostress analysis of Denizli basin (w Turkey): implications of spatial variation of relative paleostress magnitudes and orientations. J. Asian Earth Sci. 27, 207222.
Kaymakci, N., Aldanmaz, E., Langereis, C., Spell, T.L., Gurer, O.F., Zanetti, K.A., 2007. Late Miocene transcurrent tectonics in NW Turkey: evidence from palaeomagnetism and 40Ar-39Ar dating of alkaline volcanic rocks. Geol. Mag. 144 (2), 379.
Kaymakcı, N., Langereis, C.G., Özkaptan, M., Özacar, A.A., Gülyüz, E., Uzel, B., Sözbilir, H., 2018. Paleomagnetic evidence for upper plate response to a STEP fault, SW Anatolia. Earth Planet. Sci. Lett. 498, 101–115.
Kirschvink, J.L., 1980. The least-squares line and plane and the analysis of paleomagnetic data. Geophys. J. R. Astron. Soc. 62, 699–718.
Kissel, C., Laj, C., Şengör, A.M.C., Poisson, A., 1987. Paleomagnetic evidence for rotation in opposite senses of adjacent blocks in northeastern Aegea and Western Anatolia. Geophys. Res. Lett. 14 (9), 907–910.
Koçyiğit, A., Özacar, A.A., 2003. Extensional neotectonic regime through the NE edge of the outer Isparta Angle, SW Turkey: new field and seismic data. Turkish J. Earth Sci. 12 (1), 67–90.
Koçyiğit, A., Yusufoğlu, H., Bozkurt, E., 1999. Evidence from the Gediz graben for episodic two-stage extension in western Turkey. J. Geol. Soc. 156 (3), 605–616.
Kondopoulou, D., Sen, S., Aidona, E., Van Hinsbergen, D.J.J., Koufos, G., 2011. Rotation history of Chios island, Greece since the Middle Miocene. J. Geodyn. 51 (5), 327–338.
Koymans, M.R., Langereis, C.G., Pastor-Galán, D., van Hinsbergen, D.J., 2016. Paleomagnetism. org: an online multi-platform open source environment for paleomagnetic data analysis. Comput. Geosci. 93, 127–137.
Le Pichon, X., Angelier, J., 1979. The Hellenic arc and trench system: a key to the neotectonic evolution of the eastern Mediterranean area. Tectonophysics 60, 1–42.
Lips, A.L., Cassard, D., Sözbilir, H., Yilmaz, H., Wijbrans, J.R., 2001. Multistage exhumation of the Menderes massif, western Anatolia (Turkey). Int. J. Earth Sci. 89 (4), 781–792.
MTA, 2002. 1/500,000 scaled geological maps of Turkey, General Directorate of Mineral Research and Exploration, Ankara.
McFadden, P.L., McElhinny, M.W., 1988. The combined analysis of remagnetisation circles and direct observations in paleomagnetism. Earth Planet. Sci. Lett. 87, 161–172.
Meulenkamp, J.E., Wortel, M.J.R., van Wamel, W.A., Spakman, W., Hoogerduyn, Strating E., 1988. On the Hellenic subduction zone and the geodynamical evolution of Crete since the late middle Miocene. Tectonophysics 146, 203–215.
Morris, A., Anderson, M., 1996. First palaeomagnetic results from the Cycladic Massif, Greece, and their implications for Miocene extension directions and tectonic models in the Aegean. Earth Planet. Sci. Lett. 142, 397–408.
Nebert, K., 1978. Linyit iceren Soma Neojen bölgesi, Bati Anadolu. Mineral Research and Exploration Institute of Turkey (MTA) Bulletin, 90, 20–69.
Okay, A.İ., Siyako, M., 1993. The new position of the İzmir-Ankara Neo-Tethyan Suture between İzmir and Balıkesir. In: Proceedings of the Ozan Sungurlu Symposium, pp. 333–355.
Okay, A.İ., 2001. Stratigraphic and metamorphic inversions in the central Menderes Massif: a new structural model. Int. J. Earth Sci. 89, 709–727. https://doi.org/10.1007/s005310000098.
Okay, A.İ., İşintek, İ., Altıner, D., Özkan-Altıner, S., Okay, N., 2012. An olistostrome–mélange belt formed along a suture: Bornova Flysch zone, western Turkey. Tectonophysics 568, 282–295.
Özkaymak, Ç., Sözbilir, H., Uzel, B., 2013. Neogene-Quaternary evolution of the Manisa Basin: evidence for variation in the stress pattern of the İzmir-Balıkesir Transfer Zone, western Anatolia. J. Geodyn. 65, 117–135.
Passier, H.F., de Lange, G.J., Dekkers, M.J., 2001. Rock-magnetic properties and geochemistry of the active oxidation front and the youngest sapropel in the Mediterranean. Geophys. J. Int. 145, 604–614.
Paul, A., Karabulut, H., Mutlu, A.K., Salaün, G., 2014. A comprehensive and densely sampled map of shear-wave azimuthal anisotropy in the Aegean-Anatolia region. Earth Planet. Sci. Lett. 389, 14–22.
Pe-Piper, G., Piper, D.J.W., Matarangas, D., 2002. Regional implications of geochemistry and style of emplacement of Miocene I-type diorite and granite, Delos, Cyclades, Greece. Lithos 60, 47–66.
Philippon, M., Brun, J.P., Gueydan, F., 2012. Deciphering subduction from exhumation in the segmented Cycladic Blueschist Unit (Central Aegean, Greece). Tectonophysics 524–525, 116–134. https://doi.org/10.1016/j.tecto.2011.12.025.
Philippon, M., Brun, J.P., Gueydan, F., Sokoutis, D., 2014. The interaction between Aegean back-arc extension and Anatolia escape since Middle Miocene. Tectonophysics 631, 176–188. https://doi.org/10.1016/j.tecto.2014.04.039.
Purvis, M., Robertson, A., 2004. A pulsed extension model for the Neogene-Recent E-W-trending Alasehir Graben and the NE–SW-trending Selendi and Gördes Basins, Western Turkey. Tectonophysics 391, 171–201.
Purvis, M., Robertson, A.H.F., 2005. Sedimentation of the Neogene-Recent Alaşehir (Gediz) continental graben system used to test alternative tectonic models for western (Aegean) Turkey. Sed. Geol. 173, 373–408.
Ring, U., Susanne, L., Matthias, B., 1999. Structural analysis of a complex nappe sequence and late orogenic basins from the Aegean Island of Samos, Greece. J. Struct. Geol. 21, 1575–1601.
Sarı, B., 2012. Late Maastrichtian-Late Palaeocene planktic foraminiferal biostratigraphy of the matrix of the Bornova Flysch Zone around Bornova. Turkish J. Earth Sci. (in press). https://doi.org/10.3906/yer-1107-2.
Schueller, S., Gueydan, F., Davy, P., 2005. Brittle-ductile coupling: Role of ductile viscosity on brittle fracturing. Geophys. Res. Lett. 32 (10).
Schueller, S., Gueydan, F., Davy, P., 2010. Mechanics of the transition from localized to distributed fracturing in layered brittle–ductile systems. Tectonophysics 484 (1), 48–59.
Şen, S. and Seyitoğlu, G., 2009. Magnetostratigraphy of early–middle Miocene deposits from east–west trending Alaşehir and Büyük Menderes grabens in western Turkey, and its tectonic implications. In: van Hinsbergen, D.J.J., et al. (Eds.), Collision and Collapse at the Africa–Arabia–Eurasia Subduction Zone. In: Geol. Soc. (Lond.) Spec. Publ., vol. 311, pp. 321–342.
Şengör, A.M.C., 1979. The North Anatolian Transform Fault: its age, offset and tectonic significance. J. Geol. Soc. London 136, 269–282.
Şengör, A.M.C., Yılmaz, Y., 1981. Tethyan evolution of Turkey: a plate tectonic approach. Tectonophysics 75, 181–241.
Şengör, A.M.C., Görür, N., Şaroğlu, F., 1985. Strike-slip faulting and related basin formation in zones of tectonic escape: Turkey as a case study. In: Biddle, K., Christie-Blick, N. (Eds.), Strike-Slip Deformation, Basin Formation and Sedimentation. Society of Economic Paleontologists and Mineralogists, 37, 227–264.
Şengör, A.M.C., 1987. Cross-faults and differential stretching of hanging walls in regions of low-angle normal faulting: examples from western Turkey. Geol. Soc. London, Special Publications 28 (1), 575–589.
Seyitoğlu, G., Çemen, İ., Tekeli, O., 2000. Extensional folding in the Alaşehir (Gediz) Graben, western Turkey. J. Geol. Soc. Lond. 157, 1097–1100.
Seyitoğlu, G., Scott, B.C., 1996. The cause of NS extensional tectonics in western Turkey: tectonic escape vs back-arc spreading vs orogenic collapse. J. Geodyn. 22 (1–2), 145–153.
Seyitoğlu, G., Tekeli, O., Çemen, İ., Şen, Ş., Işık, V., 2002. The role of the flexural rotation/rolling hinge modeling the tectonic evolution of the Alaşehir graben, Western Turkey. Geol. Mag. 139, 15–26.
Seyitoğlu, G., Işık, V., Çemen, I., 2004. Complete tertiary exhumation history of the Menderes Massif, Western Turkey: an alternative working hypothesis. Terra Nova 16, 358–363.
Sözbilir, H., 2001. Extensional tectonics and the geometry of related macroscopic structures: field evidence from the Gediz detachment, western Turkey. Turk. J. Earth Sci. 10 (2), 51–67.
Sözbilir, H., 2002. Geometry and origin of folding in the Neogene sediments of the Gediz Graben, Western Anatolia, Turkey. Geodin. Acta 15, 277–288.
Sözbilir, H., İnci, U., Erkül, F., Sümer, Ö., 2003. An active intermittent transfer zone accommmodating N-S extension in western Anatolia and its relation to the North Anatolian Fault System. International Workshop on the North Anatolian, East Anatolian and Dead Sea Fault Systems: Recent Progress in Tectonics and Palaeoseismology and Field Training Course in Palaeoseismology, Ankara, Abstracts, 87.
Sözbilir, H., Sarı, B., Uzel, B., Sümer, Ö., Akkiraz, S., 2011. Tectonic implications of transtensional supradetachment basin development in an extension-parallel transfer zone: the Kocaçay Basin, western Anatolia Turkey. Basin Res. 23 (4), 423–448.
Sözbilir, H., Uzel, B., Sümer, Ö., Eski, S., Softa, M., Tepe, Ç., Özkaymak, Ç., Baba, A., 2017. ÇANAKKALE-AYVACIK DEPREM FIRTINASININ (14 OCAK-20 MART 2017) SİSMİK KAYNAKLARI. *Eskişehir Teknik Üniversitesi Bilim ve Teknoloji Dergisi B-Teorik*. Bilimler 6, 1–17.
Sümer, Ö., Uzel, B., Özkaymak, Ç., Sözbilir, H., 2018. Kinematics of the Havran-Balıkesir Fault Zone and its implication on geodynamic evolution of the Southern Marmara Region, NW Anatolia. Geodinamica Acta 30 (1), 306–323.
Tauxe, L., Watson, G.S., 1994. The fold test: an eigen analysis approach. Earth Planet. Sci. Lett. 122 (3), 331–341.
Tauxe, L., 2010. Essentials of paleomagnetism. Univ. of California Press. ISO 6.
Taymaz, T., Yilmaz, Y., Dilek, Y., 2007. The geodynamics of the Aegean and Anatolia: introduction. Geol. Soc. London Spec. Public. 291 (1), 1–16.
Thébault, E., Finlay, C.C., Beggan, C.D., Alken, P., Aubert, J., Barrois, O., et al., 2015. International geomagnetic reference field: the 12th generation. Earth Planets Space 67 (1), 1–19.
Tirel, C., Gautier, P., Van Hinsbergen, D.J.J., Wortel, M.J.R., 2009. Sequential development of interfering metamorphic core complexes: numerical experiments and comparison with the Cyclades, Greece. Geol. Soc. Lond., Spec. Publicat. 311 (1), 257–292.
Torsvik, T.H., Van der Voo, R., Preeden, U., Niocaill, C.M., Steinberger, B., Doubrovine, P. V., van Hinsbergen, D.J.J., Domeier, M., Gaina, C., Tovher, E., Meert, J.G., McCausland, P.J., Cocks, L.R.M., 2012. Phanerozoic polar wander, palaeogeography and dynamics Source of the Document Earth-Science Reviews 114 (3–4), 325–368.
Uzel, B., Sözbilir, H., 2008. A first record of a strike-slip basin in western Anatolia and its tectonic implication: the Cumaovası Basin. Turk. J. Earth Sci. 17 (3), 559–591.
Uzel, B., Sözbilir, H., Özkaymak, Ç., 2012. Neotectonic evolution of an actively growing superimposed basin in western Anatolia: the inner bay of İzmir Turkey. Turkish J. Earth Sci. 21 (4), 439–471.
Uzel, B., Sözbilir, H., Özkaymak, Ç., Kaymakcı, N., Langereis, C.G., 2013. Structural evidence for strike-slip deformation in the Izmir-Balıkesir transfer zone and

consequences for late Cenozoic evolution of western Anatolia (Turkey). J. Geodyn. 65, 94–116.
Uzel, B., Langereis, C.G., Kaymakci, N., Sözbilir, H., Özkaymak, Ç., Özkaptan, M., 2015. Paleomagnetic evidence for an inverse rotation history of Western Anatolia during the exhumation of Menderes core complex. Earth Planet. Sci. Lett. 414, 108–125.
Uzel, B., Sümer, Ö., Özkaptan, M., Özkaymak, Ç., Kuiper, K., Sözbilir, H., Langereis, C.G., 2017. Palaeomagnetic and geochronological evidence for a major middle Miocene unconformity in Söke Basin (western Anatolia) and its tectonic implications for the Aegean region. J. Geol. Soc. 174, 721–740.
van Hinsbergen, D.J.J., Kaymakci, N., Spakman, W., Torsvik, T.H., Amaru, M., 2010a. Reconciling geological history with mantle structure in western Turkey. Earth Planet. Sci. Lett. 297, 674–686.
Vandenberg, L.C., Lister, G.S., 1996. Structural analysis of basement tectonites from the Aegean metamorphic core complex of Ios, Cyclades, Greece. J. Struct. Geol. 18 (12), 1437–1454.
van Hinsbergen, D.J.J., Hafkenscheid, E., Spakman, W., Meulenkamp, J.E., Wortel, R., 2005. Nappe stacking resulting from subduction of oceanic and continental lithosphere below Greece. Geology 33, 325–328.
van Hinsbergen, D.J.J., Dekkers, M. J., Bozkurt, E., Koopman, M., 2010b. Exhumation with a twist: paleomagnetic constraints on the evolution of the Menderes metamorphic core complex, western Turkey. Tectonics, 29(3), TC3009, 1–33.
van Hinsbergen, D.J.J. and Schmid, S. M., 2012. Map view restoration of Aegean–West Anatolian accretion and extension since the Eocene. Tectonics, 31(5), TC5005, 1–40.
Walcott, C.R., White, S.H., 1998. Constraints on the kinematics of post-orogenic extension imposed by stretching lineations in the Aegean region. Tectonophysics 298, 155–175.
Yilmaz, Y., Genç, Ş. C., Gürer, F., Bozcu, M., Yilmaz, K., Karacik, Z., Altunkaynak, Ş., Elmas, A., 2000. When did the western Anatolian grabens begin to develop? In: Bozkurt, E., Winchester, J.A. & Piper, J.D.A. (Eds.) Tectonics and Magmatism in Turkey and the Surrounding Area. Geological Society, London, Special Publications, 173(1), 353–384.
Zhu, L., Akyol, N., Mitchell, B.J., Sözbilir, H., 2006. Seismotectonics of western Turkey from high resolution earthquake relocations and moment tensor determinations. Geophys. Res. Lett. 33, L07316. https://doi.org/10.1029/2006GL025842.
Zijderveld, J.D.A., 1967. AC demagnetization of rocks: analysis of results. In: Collinson, D.W., Creer, K.M. (Eds.), Methods in Paleomagnetism. Elsevier, Amsterdam, pp. 254–286.